PERGAMON

Journal of Quantitative Spectroscopy & Radiative Transfer 83 (2004) 15–46

Journal of Quantitative Spectroscopy & Radiative Transfer

www.elsevier.com/locate/jqsrt

A new approach to the retrieval of surface properties from earthshine measurements

Robert J.D. Spurr*

Harvard-Smithsonian Center for Astrophysics, 60 Garden Street, Cambridge, MA 02138, USA

Received 27 June 2002; accepted 9 October 2002

Abstract

Instruments such as the MODIS and MISR radiometers on EOS AM-1, and POLDER on ADEOS have been deployed for the remote sensing retrieval of surface properties. Typically, retrieval algorithms use linear combinations of semi-empirical bidirectional reflectance distribution function (BRDF) kernels to model surface reflectance. The retrieval proceeds in two steps; first, an atmospheric correction relates surface BRDF to top-of-atmosphere (TOA) reflectances, then regression is used to establish the linear coefficients used in the kernel combination. BRDF kernels may also depend on a number of physical or empirical non-linear parameters (e.g. ocean wind speed for a specular BRDF); such parameters are usually assumed known. A major source of error in this retrieval comes from lack of knowledge of planetary boundary layer (PBL) aerosol properties.

In this paper, we present a different approach to surface property retrieval. For the radiative transfer simulations, we use the discrete ordinate LIDORT model, which has the capability to generate simultaneous fields of radiances and weighting functions in a multiply scattering multi-layer atmosphere. Surface–atmosphere coupling due to multiple scattering and reflection effects is treated in full; the use of an atmospheric correction is not required. Further, it is shown that sensitivities of TOA reflectances to both linear and non-linear surface BRDF parameters may be established directly by explicit analytic differentiation of the discrete ordinate radiative transfer equations. Surface properties may thus be retrieved directly and conveniently from satellite measurements using standard non-linear fitting methods. In the fitting for BRDF parameters, lower-boundary aerosol properties can either be retrieved as auxiliary parameters, or they can be regarded as forward model parameter errors. We present examples of simulated radiances and surface/aerosol weighting functions for combinations of multi-angle measurements at several different wavelengths, and we perform some examples of self-consistent non-linear fitting to demonstrate feasibility for this kind of surface property retrieval.
Published by Elsevier Ltd.

* Tel.: +1-617-496-7819; fax: +1-617-354-3415.
E-mail address: rspurr@cfa.harvard.edu (R.J.D. Spurr).

0022-4073/04/$ - see front matter. Published by Elsevier Ltd.
doi:10.1016/S0022-4073(02)00283-2

1. Introduction

1.1. Background to BRDF retrieval

Reflectance of light from the terrestrial surfaces is an anisotropic phenomenon; it is characterized mathematically by the bidirectional reflectance distribution function (BRDF). The BRDF of a given surface depends on the incident and reflected viewing directions and also on intrinsic properties of the surface itself. Proper consideration of surface reflectance is important in remote sensing, not only for the direct retrieval of surface properties from multi-angle backscatter measurements, but also in the retrieval of atmospheric constituent distributions. Both applications require knowledge of surface BRDFs, plus accurate radiative transfer (RT) modeling to deal with surface–atmosphere coupling due to multiple scattering and reflection.

In recent years, a number of remote sensing instruments have been deployed for surface retrieval. These include the two EOS radiometers MODIS and MISR on the AM-1 platform, infrared monitors such as AVHRR and ATSR-2, and the POLDER instrument that flew on ADEOS-1. BRDF and surface albedo retrieval products have been generated on an operational basis for the MODIS instrument [1]. In these applications, a variety of semi-empirical BRDFs (kernels) have been used to model surface reflectance; kernels have been used singly or in linear combinations. The total surface BRDF is then related to the top-of-atmosphere (TOA) BRDF (as seen by the instrument) by means of an atmospheric correction determined from radiative transfer considerations.

The kernel-based BRDF model may be written as

$$\rho(\theta_s, \theta_r, \phi) = \sum_{k=1}^{K} a_k f_k(\theta_s, \theta_r, \phi; \boldsymbol{b}_k) \tag{1}$$

for the BRDF function at incident zenith angle θ_s and reflected zenith angle θ_r, with ϕ indicating the relative azimuth between the planes containing the incident and reflected beams at the point of reflection. Geometrical dependence on incident and reflected directions is assumed known for each kernel f_k. Each kernel depends non-linearly on a set $\boldsymbol{b}_k$ of parameters which characterize the kernel shape.

In the MODIS retrieval, land surface BRDF is simulated as a linear combination of three BRDF kernels [1]. Once the reflectance at the top of atmosphere (TOA) has been translated to the surface BRDF by means of an atmospheric correction, the retrieval becomes essentially a linear regression for the coefficients $\{a_1, a_2, a_3\}$ (parameters $\boldsymbol{b}_k$ are assumed known). In the POLDER work, TOA reflectances are also corrected for atmospheric effects. Surface BRDF signatures for various land surface types may then be modeled with kernel functions (either singly or in linear combinations) to determine either the coefficients a_k (linear regression) or the parameters $\boldsymbol{b}_k$ (chi-square grid-search) [2].

In reality, atmospheric correction itself is coupled to surface BRDF. Coupling effects can be separated with the assumption of a Lambertian surface in the RT simulations. Though convenient and widely used, this assumption can generate significant errors; in particular it becomes increasingly untenable for larger atmospheric optical thickness. In the MODIS BRDF retrieval, the atmospheric correction is applied iteratively. First, a correction is made using the Lambertian assumption and then the BRDF kernel coefficients are established by linear fitting. The resulting BRDF is then used

to re-compute the correction, after which a second linear regression will generate an improved set of coefficients [1]. For most applications, one such iteration is usually sufficient to reduce surface reflectance errors to below the 3% level. Additional errors in retrieval parameters are due to uncertainties in modeled atmospheric properties, the most prominent being the planetary boundary layer (PBL) aerosol distribution.

1.2. Aims of this study

In this work we adopt a much more direct approach. We will treat surface property retrieval as a standard non-linear fitting problem of the sort frequently encountered in remote sensing of the earth/atmosphere system. The forward model (radiative transfer) part of such an algorithm will simulate earthshine reflectances at the satellite, and these are to be compared directly with the instrument radiance measurements. The inversion may use unconstrained least squares or it can incorporate additional regularization either in the form of *a priori* knowledge (optimal estimation) or the use of a regularization parameter (Phillips–Tikhonov). In all methods, the retrievals proceed iteratively, with each iteration step being a linear inversion based on the minimization of a functional such as the chi-square merit function. In optimal estimation, the iteration for state vector $\boldsymbol{x}_i$ is

$$\boldsymbol{x}_{i+1} = \boldsymbol{x}_i + (\mathbf{K}^{\mathrm{T}}\mathbf{S}_{\mathrm{meas}}^{-1}\mathbf{K} + \mathbf{S}_{\mathrm{a}}^{-1})^{-1}\mathbf{K}^{\mathrm{T}}\mathbf{S}_{\mathrm{meas}}^{-1}[\mathbf{Y}_{\mathrm{meas}} - \boldsymbol{F}(\boldsymbol{x}_i) - \mathbf{K}(\boldsymbol{x}_{\mathrm{a}} - \boldsymbol{x}_i)], \tag{2}$$

in terms of the vector $\mathbf{Y}_{\mathrm{meas}}$ of earthshine reflectance measurements, the forward model simulation $\boldsymbol{F}(\boldsymbol{x}_i)$, and the Jacobian (or weighting function) matrix $\mathbf{K}(\boldsymbol{x}_i)$ of derivatives of $\boldsymbol{F}(\boldsymbol{x}_i)$ with respect to the elements in state vector $\boldsymbol{x}_i$. $\mathbf{K}^{\mathrm{T}}$ is the matrix transpose. $\boldsymbol{x}_{\mathrm{a}}$ is the *a priori* state vector, with covariance matrix $\mathbf{S}_{\mathrm{a}}$, and $\mathbf{S}_{\mathrm{meas}}$ is the error covariance on the measurement vector. For a surface property retrieval based on linear combinations of BRDF kernels, state vector $\boldsymbol{x}_i$ may consist of the linear kernel coefficients a_k or the non-linear kernel parameters $\boldsymbol{b}_k$ or any combination thereof. It may also include a number of auxiliary parameters, such as the optical properties of the PBL aerosol. For details on optimal estimation and other fitting methods, see [3].

The forward model is the key to this type of iterative retrieval. For the surface property application, we have two main requirements: (1) the RT model should have a full multiple scattering treatment in an multi-layer stratified atmosphere along with a comprehensive bidirectional treatment of surface reflectance; and (2) in addition to the usual radiance simulation $\boldsymbol{I}_{\mathrm{toa}} = \boldsymbol{F}(\boldsymbol{x})$, the RT model should have the ability to generate accurately and efficiently any sets of weighting functions $\mathbf{K}_{\mathrm{toa}}(\boldsymbol{x}) = \partial\boldsymbol{F}(\boldsymbol{x})/\partial R$, where R is any surface or atmospheric parameter to be retrieved. These requirements will ensure that atmosphere/BRDF coupling is treated in full, and that surface property sensitivity applies to radiances as seen by the remote sensing instrument; there is no need for atmospheric corrections and a two-step breakdown of the retrieval.

In this work, we use the LIDORT model [4] which has been written for these sorts of retrieval problems. LIDORT is a discrete ordinate RT package designed to deliver simultaneous fields of radiance values and all necessary Jacobian derivatives from a single call to the model. Jacobians are calculated by explicit analytic differentiation of the complete set of discrete ordinate RT equations in a multi-layer anisotropically scattering atmosphere; there is no need for time-consuming finite

difference approximations which require external perturbations of the atmospheric medium and separate calls to the (intensity-only) RT model. LIDORT will generate output at arbitrary viewing geometry and optical depth. The pseudo-spherical approximation (solar beam attenuation in a curved shell atmosphere) is standard, and there is also a sphericity correction available for wide-angle off-nadir viewing directions [5]. LIDORT was developed primarily for atmospheric retrieval applications, in particular for O_3 profile retrieval from nadir UV backscatter spectrometers. Fast 4 and 6 stream versions of LIDORT will be incorporated into the first operational ozone profile retrieval algorithm for the OMI instrument [6]. LIDORT has also been used for total vertical column retrieval of selected trace species from GOME backscatter measurements in the UV and visible [7].

A full BRDF treatment of the surface has already been developed for LIDORT, but with only one kernel function. Analytic surface property weighting functions have so far only been derived for an albedo factor which normalizes the BRDF [8]. In this work, we re-formulate and extend the surface boundary condition in terms of a linear combination of BRDF kernels. We then examine the derivation of analytic weighting functions to include derivatives with respect to *all* linear and non-linear parameters to be considered as part of a surface property retrieval. These derivations are at the heart of this work, and are found in Section 3. Lambertian albedo weighting functions have also been derived for the linearized RT model GOMETRAN [9]. Recently, an extension to non-Lambertian surface property weighting functions has been outlined in Landgraf et al. [10], using a Gauss–Seidel RT model and an adjoint perturbation-model approach to the linearization.

We present examples of simulated earthshine reflectances for a range of viewing angles and for a number of BRDF-kernel combinations, including specular reflection and various land-surface vegetation types. Computations are done for 6 wavelengths in the visible and for a number of PBL aerosol optical thickness values. Jacobian weighting functions with respect to these linear and non-linear BRDF parameters are presented, and these Jacobians are useful for examining the sensitivity of surface retrieval. We also look at PBL aerosol weighting functions with respect to optical thickness, single scattering albedo and Angstrom exponent. To demonstrate feasibility for a simultaneous retrieval of surface parameters and PBL aerosol properties using multi-angle synthetic measurements at a small number of wavelengths, we construct synthetic measurements using LIDORT, and add measurement and random noise. Since the forward model also uses LIDORT, any such "quasi-perfect" retrieval should return state vector elements close to their true values, depending on the level of noise added to the measurements. We show that this retrieval is feasible for a typical 3-kernel BRDF formulation, and for a number of values of PBL aerosol optical thickness.

The plan of the paper is straightforward. In Section 2, we summarize BRDF kernel parameterizations, including the ones used for MODIS BRDF retrieval. Here we also look at the decomposition of kernels and their parameter derivatives in terms of a Fourier series in the cosine of the relative azimuth between planes of incidence and reflection. This decomposition is an essential prerequisite for the subsequent RT analysis. In Section 3 we present the discrete ordinate theory required for the analytic determination of surface property Jacobians. This is not a complete exposition of the LIDORT model; we do not discuss atmospheric solutions to the radiative transfer equations, but instead concentrate on the surface boundary condition and the coupling of BRDFs in the radiation field. Numerical results are presented in Section 4. Following the scenario set-up in Section 4.1, Section 4.2 gives LIDORT simulations of TOA reflectance for a number of surface BRDF kernel combinations. In Section 4.3 we look at the corresponding weighting functions with respect to surface and PBL aerosol properties. In Section 4.4 we perform a self-consistent direct fitting of surface

and PBL aerosol properties. We conclude with some remarks on the implications of this study for operational retrieval of surface properties.

2. BRDF formalism

2.1. BRDF kernels used in this work

Semi-empirical BRDF models tend to be divided between those that use a volume scattering treatment by surface facets, and those that use geometric-optics modeling of various shadow effects. In these formulations, the BRDF itself usually consists of a constant Lambertian term (isotropic surface) plus a kernel function depending on the model used:

$$\rho(\theta_s, \theta_r, \phi) = a_0 + a_1 f(\theta_s, \theta_r, \phi; \boldsymbol{b}), \tag{3}$$

where $\boldsymbol{b}$ indicates a set of non-linear parameters characterizing the kernel.

Two volume scattering kernels, the Ross-thin and Ross-thick models [11], are used in MODIS BRDF retrieval models. The Ross-type BRDFs depend on the leaf-area index (LAI); the LAI parameterization is subsumed in the linear weighting factors a_0 and a_1, and the Ross kernels f_{thin} and f_{thick} are purely geometric functions free from any non-linear parameterizations. For geometric-optics vegetation models, MODIS uses the Li-sparse and Li-dense models [11]. These are based on the treatment of canopy crowns as spheroids; there are 2 non-linear parameters $b_1^{(\text{Li})}$ (crown vertical to horizontal radius) and $b_2^{(\text{Li})}$ (ratio of height of crown center above ground to vertical radius). For MODIS BRDF products, most land surfaces are modeled as the weighted sum of three kernels, one for an isotropic surface, one Ross-type kernel and one Li-type kernel. Values of $b_1^{(\text{Li})} = 1.0$ are used for the Li-sparse kernel, and $b_1^{(\text{Li})} = 2.5$ for the Li-dense kernel; $b_2^{(\text{Li})}$ is fixed at 2.0 for both Li-type kernels. The POLDER BRDF retrieval also uses a 3-kernel linear combination known as the Roujean model [2]. This has a Lambertian term, a Ross-thick volume-scattering kernel and a simple parameter-free geometric-optics kernel [12].

Other more empirically based BRDF models have been suggested for vegetation surfaces; these include the Rahman 3-parameter model [13] and the Hapke model (also 3 parameters) [14]. These models are not usually used as part of a linear kernel combination. Differences in these two models are mainly in the treatment of the so-called hot-spot function (the backscatter peak). For water surfaces, it is common to use the specular (glitter) BRDF based on a Cox–Munk Gaussian distribution of wave facets [19]; in this case wind speed and refractive index of water are the two non-linear parameters characterizing the kernel. MODIS BRDF retrieval uses a Lambertian, Cox–Munk and Li-sparse combination for certain land scenarios with a substantial surface water component (melting ice, flooded fields); the wind speed is pre-set at 5 m/s.

In this work, we consider 8 non-Lambertian kernels (2 Ross-type, 2 Li-type, Roujean, Rahman, Hapke and Cox–Munk). This covers a wide range of surface types. Mathematical expressions for these kernels are found in Appendix A, where dependencies of the kernels on non-linear parameters $\boldsymbol{b}$ are made explicit. Fig. 1 shows some kernel comparisons for viewing angles in the principal plane, with solar angles as indicated; plots of the Rahman, Cox–Munk and Hapke functions have been scaled for convenience of display. Values of non-linear parameters are as follows: $\boldsymbol{b} = \{1.0, 2.0\}$

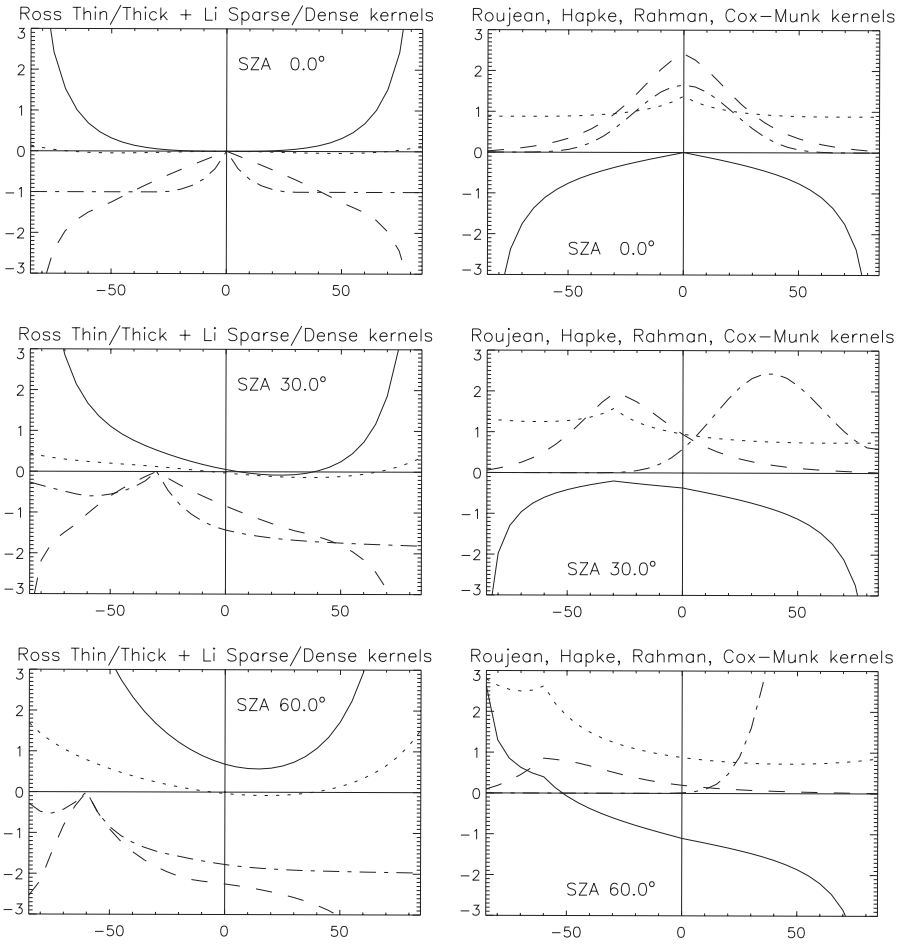

Fig. 1. (Left panels) Kernel shapes for the Ross-thin (solid line), Ross-thick (dotted), Li-sparse (dashed) and Li-dense (dash-dot) functions; (Right panels) kernel shapes for the Roujean (solid line), Hapke (dotted), Rahman (dashed) and Cox–Munk (dash-dot) functions. All results are in the principal plane for viewing angles in the range $[-85°, 85°]$.

(Li-dense); $\boldsymbol{b} = \{2.5, 2.0\}$ (Li-sparse); $\boldsymbol{b} = \{0.6, 0.06, 1.0\}$ (Hapke); $\boldsymbol{b} = \{0.1, -0.5, 1.5\}$ (Rahman); $\boldsymbol{b} = \{5.0, 1.334\}$ (Cox–Munk). For more explanation on the vector entries, refer to Appendix A.

Since we are interested in weighting functions with respect to surface quantities, we need the BRDF derivatives. Assuming the linear kernel combination in Eq. (1), we have

$$\frac{\partial \rho(\theta_s, \theta_r, \phi)}{\partial a_k} = f_k(\theta_s, \theta_r, \phi; \boldsymbol{b}_k),$$

$$\frac{\partial \rho(\theta_s, \theta_r, \phi)}{\partial b_{ck}} = \boldsymbol{a}_k \lambda_k(\theta_s, \theta_r, \phi; \boldsymbol{b}_k) \equiv \boldsymbol{a}_k \frac{\partial f_k(\theta_s, \theta_r, \phi; \boldsymbol{b}_k)}{\partial b_{ck}}.$$

Linear coefficient derivatives are easy to determine. In Appendix A, we also present explicit forms for kernel derivatives with respect to non-linear parameters b_{ck}; these are absent for the two Ross

kernels and the Roujean kernel (none of these has any free parameters). BRDF derivatives are a necessary starting point for the surface property weighting functions.

2.2. BRDF Fourier components

To solve the RT equation in an anisotropically scattering medium using the discrete ordinate method, geometrical dependence on azimuth angle is removed using a Fourier series expansion of the radiation field in terms of the cosine of the relative azimuth angle between the line-of-sight plane and the solar plane. This applies not only to the scattering field and its weighting function derivatives, but also to the bidirectional reflection function. Thus for each BRDF kernel, we have

$$f(\theta_s, \theta_r, \phi; \boldsymbol{b}_k) = \sum_{m=0}^{M} f_k^m(\theta_s, \theta_r, \boldsymbol{b}_k) \cos m\phi. \tag{4}$$

Fourier coefficients may be determined from the inverse relation

$$f^m(\theta_s, \theta_r, \boldsymbol{b}) = \frac{1+\delta_{m0}}{2\pi} \int_0^{2\pi} f(\theta_s, \theta_r, \phi; \boldsymbol{b}) \cos m\phi \, \mathrm{d}\phi. \tag{5}$$

In general the inversion must be done numerically for all values of the incident and reflected angles required in the radiative transfer computations. It is possible to use a double quadrature scheme over the intervals $[-\pi, 0]$ and $[0, \pi]$. Care needs to be taken for geometries close to hot-spot conditions; in these cases one should use a finer quadrature or resort to fine-grid trapezium rule integration. The accuracy of this implementation was tested by reconstructing the original kernels from their Fourier coefficients, up to a certain level of accuracy. For incident and reflected angles from 0° to 89° and for all values of ϕ, a quadrature with 360 terms or a trapezium integration with resolution 0.5° is sufficient to reproduce virtually all kernels to an accuracy of 10^{-4}. The main exception was found for the Cox–Munk kernel at angles of glancing incidence and reflection. We note in passing that a 25-stream quadrature rule is standard in DISORT for the BRDF decomposition [15].

The non-linear parameter derivatives $\lambda_k(\theta_s, \theta_r, \phi; \boldsymbol{b}_k)$ as defined above also have a Fourier series decomposition in cosine azimuth, and the Fourier components are established in the same way by numerical integration:

$$\lambda_k^m(\theta_s, \theta_r, \boldsymbol{b}_k) = \frac{1+\delta_{m0}}{2\pi} \int_0^{2\pi} \lambda_k(\theta_s, \theta_r, \phi; \boldsymbol{b}_k) \cos m\phi \, \mathrm{d}\phi. \tag{6}$$

The coefficient forms $f_k^m(\theta_s, \theta_r, \boldsymbol{b}_k)$ and $\lambda_k^m(\theta_s, \theta_r, \boldsymbol{b}_k)$ are basic inputs to the LIDORT computation of the mth Fourier component of the radiance and Jacobian fields. Once the kernel form is written down explicitly and its derivative found by analytic means, then the stage is set for the analytic derivation of surface property Jacobians.

There is one other constraint that should be placed on the BRDF. We take the total spherical albedo of the surface to lie between 0 and 1, that is

$$0 < \sum_{k=1}^{K} a_k S_k < 1, \quad \text{where } S_k = \frac{1}{4} \int_0^1 \int_0^1 \mu_s \mu_r f_k^0(\mu_s, \mu_r) \, \mathrm{d}\mu_s \, \mathrm{d}\mu_r \tag{7}$$

with $\mu_s = \cos\theta_s$ and $\mu_r = \cos\theta_r$.

3. BRDFs in LIDORT: analytic surface property Jacobians

For satellite applications we are interested in top of the atmosphere (TOA) upwelling radiative transfer output. In terms of the Fourier expansion in cosine azimuth as noted above, and for output at stream direction μ, we require

$$I^+_{\rm toa}(\mu,\phi) = \sum_{m=0}^{2N-1} I^m_{\rm toa}(\mu)\cos m\phi, \tag{8}$$

$$\frac{\partial I^+_{\rm toa}}{\partial R}(\mu,\phi) = \sum_{m=0}^{2N-1} \frac{\partial I^m_{\rm toa}(\mu)}{\partial R}\cos m\phi. \tag{9}$$

In the RT calculation, the maximum number of Fourier coefficients that can be used is $2N-1$, where N_s is the number of discrete ordinate polar angles used in the scattering quadrature. In practice, it is not necessary to compute all terms in the Fourier series; the summation is stopped when the addition of one more Fourier component fails to change the radiance by more than a pre-specified small "accuracy" threshold (0.001 is typical) for all output angles. It follows that one should not pre-calculate all possible BRDF Fourier coefficients, but instead evaluate them one component at a time as they are needed. From now on we assume that the Fourier decomposition holds and the Fourier index m is implied.

3.1. The discrete ordinate radiance solution at TOA

In a multi-layer atmosphere, the upwelling radiance in direction μ at TOA is

$$I^+_{\rm toa}(\mu) = H^+(\mu)T_n(\mu) + \sum_{p=1}^{n} \Lambda^+_p(\mu)T_{p-1}(\mu), \tag{10}$$

where $T_p(\mu)$ is the *cumulative* transmittance along direction μ from TOA to the lower boundary of layer $p, T_0(\mu) \equiv 1$, and $T_n(\mu)$ is the whole-atmosphere transmittance. $\Lambda^+_p(\mu)$ are the upwelling whole-layer scattered light source terms, while $H^+(\mu)$ is the upwelling intensity at the surface. An expression for $H^+(\mu)$ will be given shortly when we consider the surface boundary condition, but first we derive the layer source terms $\Lambda^+_p(\mu)$.

In the discrete ordinate method, multiple scatter integrals are approximated by a quadrature sum over a set of polar angle cosines (the discrete ordinates) selected using a double Gauss–Legendre scheme over the intervals $[-1,0]$ and $[0,1]$. Solution of the homogeneous RTE proceeds via eigenvalue methods, and the particular RTE solution (due to scattering out of the direct solar beam) is then determined by substitution or by Green's function methods. The precise forms of the homogeneous and particular solutions do not concern us here, and the reader is referred to the literature for details (see for example [16]). In an atmosphere assumed to be stratified in the vertical, the $2N$-stream discrete ordinate solution of the RTE in a given layer p is

$$I^\pm_{jp}(x) = \sum_{\alpha=1}^{N} [L_{p\alpha}X^\pm_{jp\alpha}\mathrm{e}^{-\nu_{p\alpha}x} + M_{p\alpha}X^\mp_{jp\alpha}\mathrm{e}^{-\nu_{p\alpha}(\Delta_p-x)}] + G^\pm_{jp}(x), \tag{11}$$

where $X^{\pm}_{jp\alpha}$ are the eigensolutions of the homogeneous RT equation in layer p for discrete ordinates $\mu_{\pm j}$, with corresponding separation constants $\nu_{p\alpha}$ (eigensolutions are labeled by index α), and $G^{\pm}_{jp}(x)$ are the particular RT solutions for scattering of the solar beam. x is the vertical coordinate (optical thickness measured from top of layer), with Δ_p the complete layer optical thickness. $L_{p\alpha}$ and $M_{p\alpha}$ are integration constants to be established from the imposition of boundary conditions; we discuss these in Section 3.2.

Determination of the layer source terms follows the source function integration method first outlined by Chandrasekhar [17]. Essentially, we substitute solution (11) in the multiple scatter integral which forms part of the RT equation for radiance at arbitrary polar direction, and carry out an optical thickness integration over the whole layer. The result is

$$\Lambda^{+}_{p}(\mu) = \sum_{\alpha=1}^{N} [L_{p\alpha} Y^{+}_{p\alpha}(\mu) + M_{p\alpha} Y^{-}_{p\alpha}(\mu)] + G^{+}_{p}(\mu), \tag{12}$$

where functions $Y^{\pm}_{p\alpha}(\mu)$ arise from source function integration of eigensolutions $\boldsymbol{X}^{\pm}_{p\alpha}$, and $G^{+}_{p}(\mu)$ is made up of integrations of primary scattering and direct beam contributions. Again the exact forms of these functions do not concern us here, and we assume they are known, already calculated as part of the LIDORT package (for details, see [8]). The important point is that the source terms are a linear combination of the integration constants, and we may substitute (12) in (10) to get

$$I^{+}_{\mathrm{toa}}(\mu) = H^{+}(\mu) T_n(\mu) + \sum_{p=1}^{n} T_{p-1}(\mu) \left\{ \sum_{\alpha=1}^{N} [L_{p\alpha} Y^{+}_{p\alpha}(\mu) + M_{p\alpha} Y^{-}_{p\alpha}(\mu)] + G_p(\mu) \right\}. \tag{13}$$

We seek the derivatives of $I^{+}_{\mathrm{toa}}(\mu)$ with respect to a surface property R. This may be a Lambertian albedo, a kernel factor a_k or one of the non-linear kernel parameters b_{ck}. We keep the discussion general at this point. We note that the layer homogeneous and particular RTE solutions and the corresponding source function integration terms in (12) have no dependence on surface properties, so their derivatives with respect to R vanish. Indeed TOA radiance is coupled to the surface reflectance not only directly through the surface term $H^{+}(\mu)$ but also indirectly through the integration constants $L_{p\alpha}$ and $M_{p\alpha}$. Differentiation of (13) yields

$$\frac{\partial I^{+}_{\mathrm{toa}}(\mu)}{\partial R} = \frac{\partial H^{+}(\mu)}{\partial R} T_n(\mu) + \sum_{p=1}^{n} T_{p-1}(\mu) \left[\sum_{\alpha=1}^{N} \frac{\partial L_{p\alpha}}{\partial R} Y^{+}_{p\alpha}(\mu) + \frac{\partial M_{p\alpha}}{\partial R} Y^{-}_{p\alpha}(\mu) \right]. \tag{14}$$

We now discuss derivations of the integration constants in our examination of the boundary value problem.

3.2. The boundary value problem

We keep the discussion at a general level, but omit details of the atmospheric layer calculations. The three boundary conditions are (1) downward diffuse radiation at TOA is zero; (2) upwelling and downwelling fields are continuous at atmospheric layer interfaces; (3) there exists a relation between the upwelling and downwelling fields at the surface in terms of a specified surface reflectance property. There are n layers in total. Writing the $2N$-vector $\boldsymbol{Q}_p$ for the set of unknowns $\{L_{p\alpha}, M_{p\alpha}\}$

in layer p we may write the three conditions symbolically as

$$\boldsymbol{A}_1\boldsymbol{Q}_1 = \boldsymbol{E}^{(1)} \qquad \text{for } p=1, \tag{15}$$

$$\boldsymbol{B}_p\boldsymbol{Q}_p + \boldsymbol{C}_p\boldsymbol{Q}_{p-1} = \boldsymbol{E}_p^{(2)} \quad \text{for } p=2,\ldots,n, \tag{16}$$

$$\boldsymbol{D}_n\boldsymbol{Q}_n = \boldsymbol{E}^{(3)} \qquad \text{for } p=n, \tag{17}$$

where matrices $\boldsymbol{A}_1$ and $\boldsymbol{D}_n$ have dimensions $N\times 2N$, matrices $\boldsymbol{B}_p$ and $\boldsymbol{C}_p$ for $p=2,\ldots,n$ each have dimensions $2N\times 2N$. $\boldsymbol{E}^{(1)}$ and $\boldsymbol{E}^{(3)}$ are N-vectors, $\boldsymbol{E}_p^{(2)}$ for $p=2,\ldots,n$ are $2N$-vectors.

Vectors and matrices for the first two boundary conditions are constructed from the layer RT solutions; they do not depend on surface reflection. Again we do not need to know the exact forms here; details may be found in the literature, for example in Thomas and Stamnes [16]. Explicit forms for $\boldsymbol{D}_n$ and $\boldsymbol{E}^{(3)}$ will be given in the next section. For now we note that these three conditions may be combined to produce the linear matrix algebra problem $\mathscr{A}\mathscr{Q}=\mathscr{E}$. Matrix $\mathscr{A}$ has a sparse tridiagonal block form, and its inverse may be found by standard numerical methods. (For a visualization of this matrix, see [8]). Indeed, determining the inverse $\mathscr{A}^{-1}$ is the most time-consuming part of any numerical implementation of the discrete ordinate theory in a multi-layer atmosphere. From this system, we get $\mathscr{Q}=\mathscr{A}^{-1}\mathscr{E}$ for the constants of integration, and at this juncture, we can complete the layer discrete ordinate solutions and the source function terms Λ_p required for an upward integration.

Differentiation of the above three boundary conditions gives us

$$\boldsymbol{A}_1\frac{\partial\boldsymbol{Q}_1}{\partial R} = 0 \qquad \text{for } p=1, \tag{18}$$

$$\boldsymbol{B}_p\frac{\partial\boldsymbol{Q}_p}{\partial R} + \boldsymbol{C}_{p-1}\frac{\partial\boldsymbol{Q}_{p-1}}{\partial R} = 0 \quad \text{for } p=2,\ldots,n, \tag{19}$$

$$\boldsymbol{D}_n\frac{\partial\boldsymbol{Q}_n}{\partial R} = \boldsymbol{E}'^{(3)} = \frac{\partial\boldsymbol{E}^{(3)}}{\partial R} \qquad \text{for } p=n, \tag{20}$$

where we have written $\partial\boldsymbol{Q}_p/\partial R$ for the vector of derivatives $\{\partial L_{p\alpha}/\partial R, \partial M_{p\alpha}/\partial R\}$. Clearly the solution of the new system is $\partial\mathscr{Q}/\partial R = \mathscr{A}^{-1}\mathscr{E}'$. Matrix inverse $\mathscr{A}^{-1}$ has already been established during the determination of the original set of integration constants, so the solution for the derivatives is merely a matter of back-substitution using a different right-hand vector $\mathscr{E}'$ for which the only non-zero entries are the derivatives of $\boldsymbol{E}^{(3)}$ in the boundary layer.

Thus we have solved the boundary value problem for the integration constants and their derivatives. It remains now to consider explicit forms for the matrix $\boldsymbol{D}_n$, the vectors $\boldsymbol{E}^{(3)}$ and $\boldsymbol{E}'^{(3)}$ and the surface term $H^+(\mu)$ and its derivative. To do this we look at the surface boundary condition.

3.3. Details of the BRDF surface boundary condition

The surface boundary condition is

$$H^+(\mu) = (1+\delta_{m0})\int_0^1 \rho(\mu,\mu')H^-(\mu')\,\mathrm{d}\mu' + T_\odot\rho(\mu,\mu_0), \tag{21}$$

where $H^{\pm}$ are the upwelling(+) and downwelling(−) radiance fields at the surface, and $T_{\odot}$ is the direct (solar) beam transmittance to the surface. The integral in (21) is approximated by the discrete ordinate quadrature. We first insert quadrature values μ_i in (21):

$$H_i^+ = \gamma \sum_{j=1}^{N} \mu_j w_j H_j^- \sum_{k=1}^{K} a_k f_{kij} + T_{\odot} \sum_{k=1}^{K} a_k f_{ki0}, \tag{22}$$

where we have the following definitions for BRDF kernel Fourier components at quadrature angles:

$$f_{kij} = f_k(\mu_i, \mu_j, \boldsymbol{b}_k) \quad \text{quadrature incidence, quadrature reflected,}$$

$$f_{ki0} = f_k(\mu_i, \mu_0, \boldsymbol{b}_k) \quad \text{direct beam incidence, quadrature reflected.}$$

In terms of the discrete ordinate solution (11) at the lower boundary of layer n, we have

$$H_j^{\pm} = \sum_{\alpha=1}^{N} [L_{n\alpha} X_{jn\alpha}^{\pm} \Theta_{n\alpha} + M_{n\alpha} X_{jn\alpha}^{\mp}] + G_{jn}^{\pm}(\Delta_n) \quad \text{for } j = 1, \ldots, N, \tag{23}$$

where $\Theta_{n\alpha} = \exp[-\nu_{n\alpha}\Delta_n]$ and the particular solution $G_{jn}^{\pm}$ is evaluated for the whole layer optical thickness Δ_n. Substituting these solutions in (22), we find

$$\sum_{\alpha=1}^{N} [L_{n\alpha} D_{i\alpha}^+ + M_{n\alpha} D_{i\alpha}^-] = E_i^{(3)} \quad \text{for } i = 1, \ldots, N, \tag{24}$$

where

$$D_{i\alpha}^+ = \Theta_{n\alpha} \left[X_{in\alpha}^+ - \sum_{k=1}^{K} a_k U_{ki\alpha}^+ \right], \tag{25}$$

$$D_{i\alpha}^- = X_{in\alpha}^- - \sum_{k=1}^{K} a_k U_{ki\alpha}^-, \tag{26}$$

$$E_i^{(3)} = -\left[G_{in}^+(\Delta_n) - \sum_{k=1}^{K} a_k W_{ki} \right] + T_{\odot} \sum_{k=1}^{K} a_k f_{k\mu 0}, \tag{27}$$

with the following auxiliary definitions:

$$U_{ki\alpha}^{\pm} = (1 + \delta_{m0}) \sum_{j=1}^{N} \mu_j w_j X_{jn\alpha}^{\mp} f_{kij}, \tag{28}$$

$$W_{ki} = (1 + \delta_{m0}) \sum_{j=1}^{N} \mu_j w_j G_{jn}^-(\Delta_n) f_{kij}. \tag{29}$$

In (10) we require the upwelling surface field for arbitrary polar direction μ; application of the boundary condition (21) and the discrete ordinate approximation yields

$$H^+(\mu) = (1+\delta_{m0})\sum_{j=1}^{N}\mu_j w_j H_j^- \sum_{k=1}^{K} a_k f_{k\mu j} + T_\odot \sum_{k=1}^{K} a_k f_{k\mu 0}, \tag{30}$$

where we have the following definitions for BRDF kernel Fourier components for reflection at off-quadrature angles:

$f_{k\mu i} = f_k(\mu_i, \mu, \boldsymbol{b}_k)$ quadrature incidence, user-angle reflected,

$f_{k\mu 0} = f_k(\mu, \mu_0, \boldsymbol{b}_k)$ direct beam incidence, user-angle reflected.

This completes the explicit determination of terms in the surface boundary condition. We now look at the derivatives of these terms and follow this up with the analytic determination of TOA weighting functions.

3.4. TOA weighting functions from the linearized BRDF condition

We wish to compute derivatives of the surface boundary condition. There are two choices, (1) with respect to kernel factors a_k; (2) with respect to components b_{kc} of the vector of non-linear kernel parameters.

3.4.1. Linearization w.r.t. kernel factors a_k

This is straightforward; we take the derivative of (24) and use definition (27) to obtain

$$\sum_{\alpha=1}^{N}\left[\frac{\partial L_{n\alpha}}{\partial a_k} D_{i\alpha}^+ + \frac{\partial M_{n\alpha}}{\partial a_k} D_{i\alpha}^-\right] = W_{ki} + T_\odot f_{ki0} + \sum_{\alpha=1}^{N}[L_{n\alpha}\Theta_{n\alpha}U_{ki\alpha}^+ + M_{n\alpha}U_{ki\alpha}^-]. \tag{31}$$

This equation completes the boundary value specification for the derivatives of the integration constants, and we solve for them using back-substitution as indicated above. Once this is done, we differentiate the surface upwelling radiation field at arbitrary μ as given in (22) to get

$$\frac{\partial H^+(\mu)}{\partial a_k} = (1+\delta_{m0})\sum_{j=1}^{N}\mu_j w_j \left[\frac{\partial H_i^-}{\partial a_k}\sum_{k=1}^{K} a_k f_{k\mu j} + H_j^- f_{k\mu j}\right] + T_\odot f_{k\mu 0}, \tag{32}$$

in which the derivatives of the downwelling discrete ordinate field are given by

$$\frac{\partial H_j^-}{\partial a_k} = \sum_{\alpha=1}^{N}\left[\frac{\partial L_{n\alpha}}{\partial a_k}\Theta_{n\alpha}X_{in\alpha}^- + \frac{\partial M_{n\alpha}}{\partial a_k}X_{in\alpha}^+\right]. \tag{33}$$

Eq. (32) is the end point of the chain of differentiation, and this result together with the integration constant derivatives is enough to generate the desired weighting functions at the top of the atmosphere.

3.4.2. Linearization w.r.t. kernel parameters b_{kc}

This is a little more tricky but the principles are the same. We express the linearization in terms of the derivatives of the kernel Fourier components, that is

$$\lambda_{ckij} = \frac{\partial f_{kij}(\boldsymbol{b}_k)}{\partial b_{kc}} \quad \text{quadrature incidence, quadrature reflected,}$$

$$\lambda_{cki0} = \frac{\partial f_{ki0}(\boldsymbol{b}_k)}{\partial b_{kc}} \quad \text{direct-beam incidence, quadrature reflected,}$$

$$\lambda_{ckiu} = \frac{\partial f_{kiu}(\boldsymbol{b}_k)}{\partial b_{kc}} \quad \text{quadrature incidence, user-angle reflected,}$$

$$\lambda_{cku0} = \frac{\partial f_{ku0}(\boldsymbol{b}_k)}{\partial b_{kc}} \quad \text{direct-beam incidence, user-angle reflected.}$$

These quantities may be determined from expressions in Section 2, with explicit forms for the kernel derivatives given in Appendix A. Differentiation of the boundary condition gives

$$\sum_{\alpha=1}^{N} \left[\frac{\partial L_{n\alpha}}{\partial b_{kc}} D_{i\alpha}^{+} + \frac{\partial M_{n\alpha}}{\partial b_{kc}} D_{i\alpha}^{-} \right] = \frac{\partial E_i^{(3)}}{\partial b_{kc}}. \tag{34}$$

This is in the correct form to be used in the solution of the integration constant derivatives. We have

$$\frac{\partial E_i^{(3)}}{\partial b_{kc}} = a_k \frac{\partial W_i}{\partial b_{kc}} - a_k \sum_{\alpha=1}^{N} \left[L_{n\alpha} \Theta_{n\alpha} \frac{\partial U_{ki\alpha}^{+}}{\partial b_{kc}} + M_{n\alpha} \frac{\partial U_{ki\alpha}^{-}}{\partial b_{kc}} \right] + T_{\odot} a_k \lambda_{cki0}. \tag{35}$$

From the definitions, we have for the derivatives

$$\frac{\partial U_{ki\alpha}^{\pm}}{\partial b_{kc}} = (1+\delta_{m0}) \sum_{j=1}^{N} \mu_j w_j X_{-jn\alpha}^{\mp} \lambda_{kij}, \tag{36}$$

$$\frac{\partial W_{ki}}{\partial b_{kc}} = (1+\delta_{m0}) \sum_{j=1}^{N} \mu_j w_j G_{jn}^{-}(\Delta_n) \lambda_{kij}. \tag{37}$$

For the user-defined directions, we linearize (30) in the same way:

$$\frac{\partial H^{+}(\mu)}{\partial b_{kc}} = (1+\delta_{m0}) \sum_{j=1}^{N} \mu_j w_j \left[\frac{\partial H_i^{-}}{\partial b_{kc}} \left[\sum_{k=1}^{K} a_k f_{k\mu j} \right] + H_j^{-} a_k \lambda_{k\mu j} \right] + T_{\odot} a_k \lambda_{ku0}, \tag{38}$$

with

$$\frac{\partial H_j^{-}}{\partial b_{kc}} = \sum_{\alpha=1}^{N} \left[\frac{\partial L_{n\alpha}}{\partial b_{kc}} \Theta_{n\alpha} X_{jn\alpha}^{-} + \frac{\partial M_{n\alpha}}{\partial b_{kc}} X_{jn\alpha}^{+} \right], \tag{39}$$

by analogy to Eq. (33).

3.5. Summary

In this section we have shown that, once the discrete ordinate solution for intensity has been found, it is entirely differentiable with respect to any non-linear or linear surface BRDF parameter. It follows that analytic expressions can be written down for the corresponding TOA weighting functions. Although the theory presented here applies to the satellite application, it is possible to write down analytic surface-parameter weighting functions for upwelling and downwelling radiation anywhere in the atmosphere. This has been done in the LIDORT package, which now offers complete surface weighting function capability along with the output of weighting functions with respect to atmospheric quantities. It is also possible to derive surface property weighting functions in the presence of surface emission (reflectance and emittance are related according to Kirchhoff's law). This was done for a Lambertian surface in the original LIDORT formulation [4]; the extension to a full BRDF treatment is straightforward and has been implemented in the software. Note that this formulation with surface emission also includes a weighting function with respect to the surface Planck function. Finally we note that numerical implementation of all weighting functions in LIDORT may be tested by making separate calls to the model in order to determine finite difference estimates of the Jacobian derivatives.

4. Results: LIDORT simulations and retrieval feasibility

4.1. BRDF and PBL scenarios

We assume the atmosphere to be vertically stratified, with 19 pressure levels separating 18 optically uniform layers (the levels are at $0.1, 0.3, 0.5, 1.0, 2.0, 5.0, 7.0, 10.0, 20.0, 30.0, 50.0, 70.0, 100.0, 150.0, 200.0, 300.0, 500.0, 705.0,$ and 1000.0 mb). The PBL is about 3 km thick in this stratification. The temperature distribution has been interpolated from a USA standard atmosphere. Molecular scattering coefficients and depolarization ratios are taken from empirical formulae [18]. Background LOWTRAN aerosol data are used for all layers except the lowest (PBL). For this, we assume (i) a constant aerosol single scatter albedo ω_0, (ii) a constant asymmetry parameter g_0 to be used for the aerosol phase function characterization, and (iii) a power-law relationship for the wavelength dependence of the PBL optical thickness $\delta^{(\mathrm{PBL})}(\lambda)$:

$$\delta^{(\mathrm{PBL})}(\lambda) = \delta_0^{(\mathrm{PBL})} \left[\frac{\lambda}{\lambda_0}\right]^{\gamma}, \tag{40}$$

for Angstrom exponent γ and reference wavelength $\lambda_0 = 550$ nm, with $\delta_0^{(\mathrm{PBL})} \equiv \delta^{(\mathrm{PBL})}(\lambda_0)$. We assume a Henyey–Greenstein form for the aerosol phase function, with corresponding Legendre expansion coefficients $\beta_l^{(\mathrm{PBL})}$ expressed as powers of g_0.

LIDORT requires as input the layer total optical thickness, single scatter albedo and total phase function Legendre moments. For the PBL, the first two of these are

$$\Delta^{(\mathrm{PBL})}(\lambda) = \delta^{(\mathrm{Ray})}(\lambda) + \delta^{(\mathrm{PBL})}(\lambda) \quad \text{and} \quad \Omega^{(\mathrm{PBL})}(\lambda) = \frac{\delta^{(\mathrm{Ray})}(\lambda) + \omega_0 \delta^{(\mathrm{PBL})}(\lambda)}{\Delta^{(\mathrm{PBL})}(\lambda)}, \tag{41}$$

where $\delta^{(\mathrm{Ray})}(\lambda)$ is the molecular scattering optical thickness. Similarly $\beta_l^{(\mathrm{PBL})}$ will be expressed as a combination of molecular and aerosol coefficients weighted by their respective scattering optical thickness values.

We use LIDORT to calculate TOA reflectances and their derivatives with respect to surface and PBL aerosol parameters. Jacobians for BRDF linear and non-linear parameters are calculated using the theory of the previous section, based on linear and non-linear parameterizations of the surface BRDF in terms of kernel combinations. For the PBL aerosol, we want weighting functions with respect to 3 quantities $\xi_1 = \delta_0^{(\mathrm{PBL})}$, $\xi_2 = \omega_0$ and the Angstrom exponent $\xi_3 = \gamma$. From the above definitions (41), it is straightforward to write down the derivatives $\partial\Omega^{(\mathrm{PBL})}/\partial\xi_q, \partial\Delta^{(\mathrm{PBL})}/\partial\xi_q$ and $\partial\beta_l^{(\mathrm{PBL})}/\partial\xi_q$ for $q = 1,2,3$; once these are known, we can initiate the linearization. Details of the calculation of atmospheric profile weighting functions may be found in [8].

4.2. Simulation of TOA reflectances

In Figs. 2–5, we show some simulations of earthshine reflectance for a number of BRDF kernel combinations as indicated. All calculations in this and the following section were done with an 8-stream discretization of the polar angle in the half-space $[0, \pi/2]$. All results here were calculated for PBL aerosol quantities $\gamma = 1.1$, $\omega_0 = 0.9$, $g_0 = 0.7$. The 8 sub-plots correspond to calculations done with different values of the PBL aerosol optical thickness (AOT) ($\delta_0 = 0.01, 0.05, 0.1, 0.2, 0.4, 0.7, 1.0, 2.0$). In all cases the solar zenith angle was taken at 25°, and all calculations were done in the principal plane. Linear kernel coefficients a_k and non-linear BRDF parameters $\boldsymbol{b}_k$ are indicated in the figure captions. Each plot contains results for 6 different wavelengths (360, 390, 440, 490, 540 and 590 nm) covering part of the UV and visible.

There are a number of features of interest. In Fig. 2, non-linear parameters in the Rahman BRDF kernel (see Appendix A) have a strong effect on the TOA reflectance signature at all wavelengths, and especially for small values of δ_0. The backscatter hot-spot is particularly strong; this is not surprising as an asymmetry value of -0.8 was chosen for the non-linear kernel parameter that characterizes the surface facet scattering. Fig. 3 shows TOA backscatter in the presence of specular glitter without shadow effects. Here, we take the usual Cox–Munk empirical relation $\sigma^2 = 0.003W + 0.00512$ between the wind speed W in m/s and the variance σ^2 of the Gaussian distribution of wave facet slopes. Figs. 4 and 5 show TOA reflectances for two of the kernel combinations used in MODIS BRDF retrieval studies. Non-linear kernel parameters are those assumed for the MODIS BRDF retrieval [1]. In both cases, the viewing angle dependence shows distinctive shapes; in particular note the two peaks in Fig. 5 corresponding to dominant specular glitter effects (forward direction) and dominant hot-spot backscatter. The radiance dependency on viewing angles is similar for higher wavelengths in the regime dominated by aerosol scattering, where there is a relatively smooth and slow-varying dependence of optical properties on wavelength. However, for the lower (UV) wavelengths, the effect of molecular scattering is correspondingly greater. We also note that most of the characteristic surface features are obscured for an optically thick PBL aerosol; indeed the extreme case $\delta_0 = 2.0$ is similar to a cloud deck.

4.3. Simulation of TOA weighting functions

In this section we present some graphs of weighting function output from the LIDORT model. The BRDF kernel combinations in Figs. 6–9 are the same as those used in the intensity-only simulations

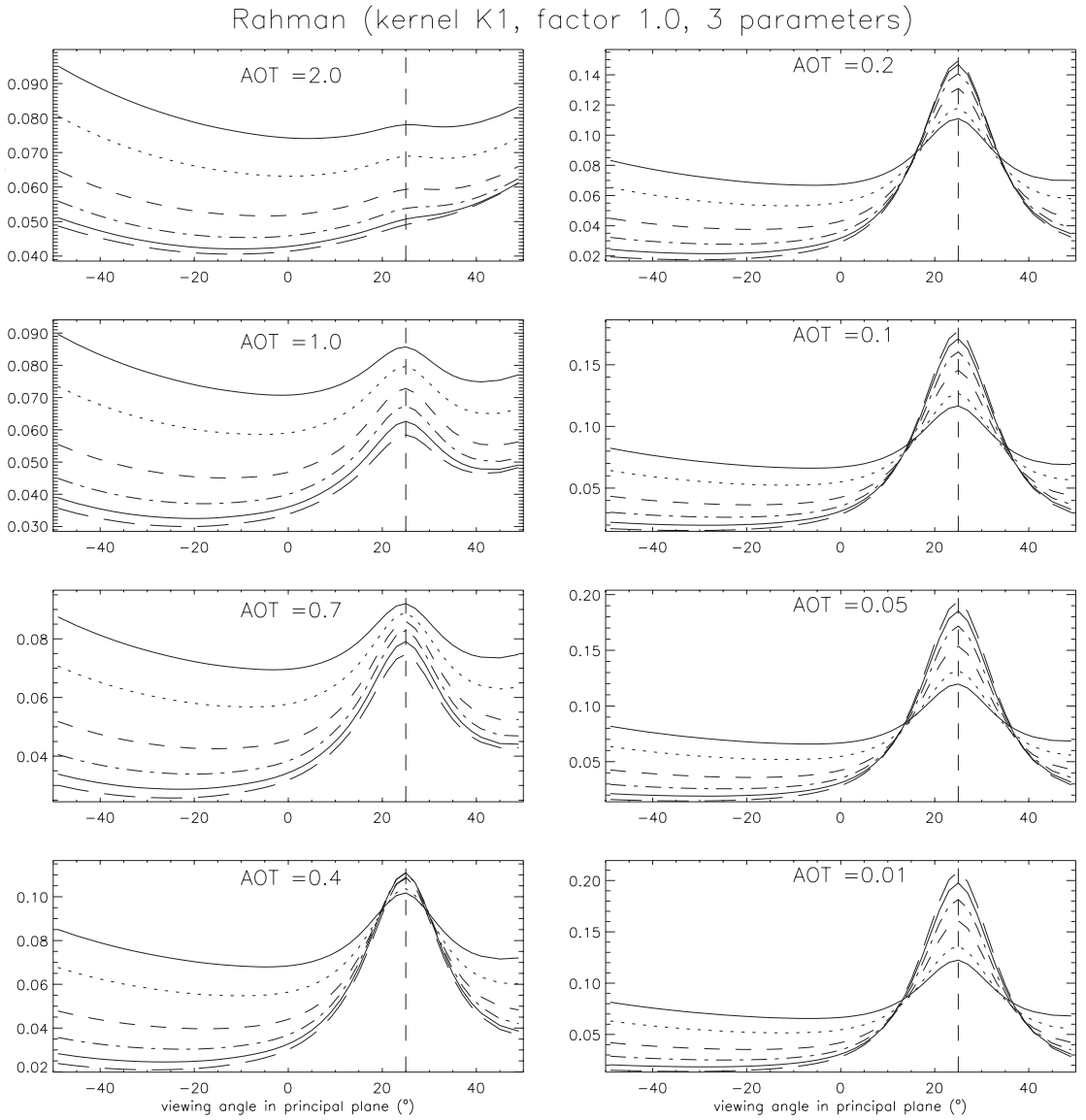

Fig. 2. Values of TOA backscatter intensity for a single BRDF kernel (the Rahman function) with linear factor 1.0, and non-linear parameters $0.1, -0.8$ (the phase function asymmetry factor) and 1.5. Values of AOT are as indicated. The strong hot-spot dependency around the solar angle (marked with the straight dashed vertical line) is evident. In the top left panel, wavelengths are in descending order from 360 nm (solid line), 390 nm (dotted line), through 440, 490, 540 and 590 nm.

of Figs. 2–5. Linear kernel scaling factors are indicated in the figure captions. Non-linear parameters are the same as those used in the previous set of figures. The set of 6 wavelengths is the same, as is the solar zenith angle and the principal plane geometry. All results in these figures are computed for an AOT value of 0.1. In all cases, weighting functions for the above-mentioned three PBL aerosol

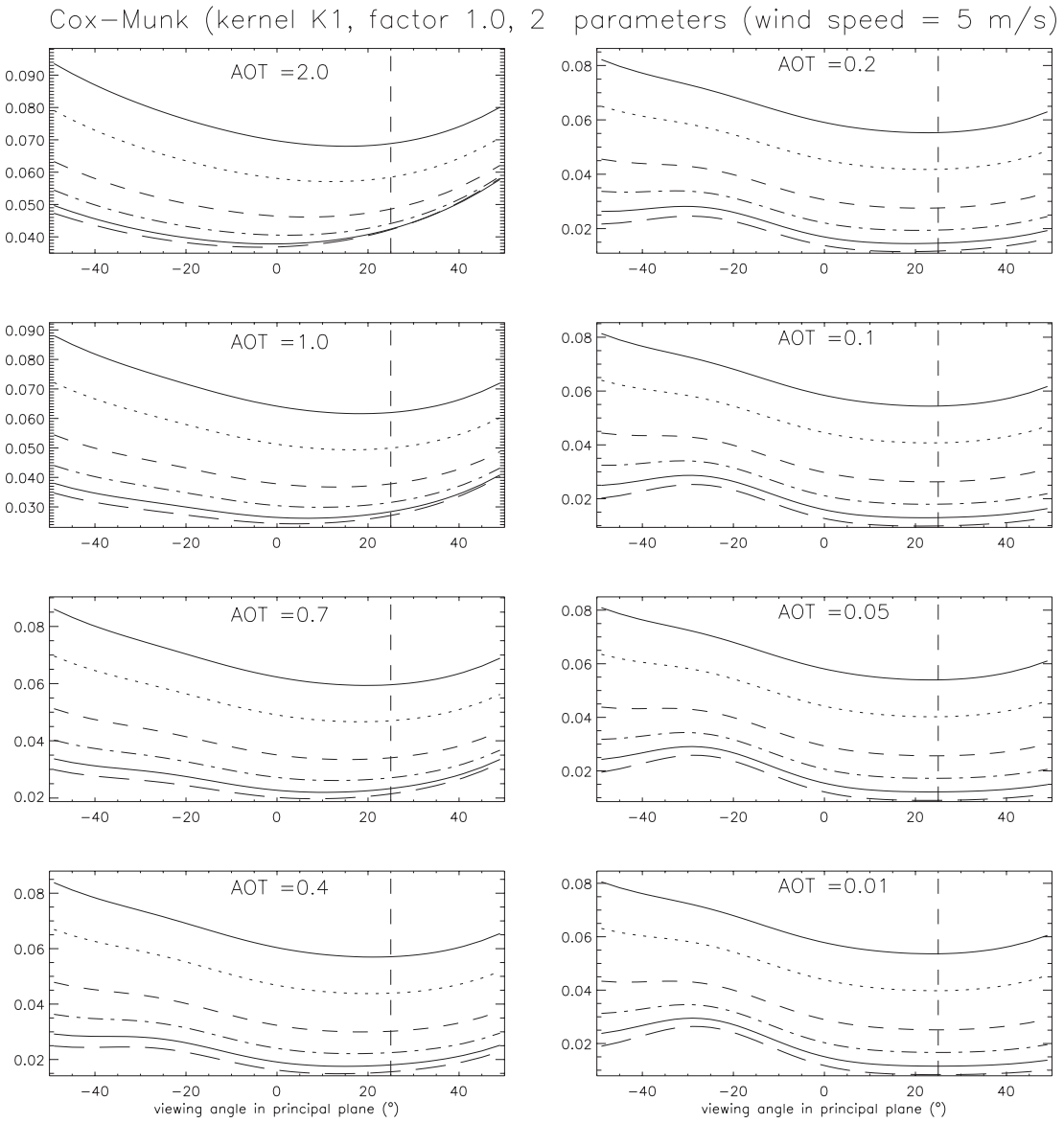

Fig. 3. Values of TOA backscatter intensity for the single Cox–Munk BRDF kernel with linear factor 1.0, and non-linear parameters 5.0 (wind speed in m/s) and 1.334 (refractive index). Wavelengths and solar zenith angle as in previous figure.

parameters are displayed. All weighting functions are parameter-normalized, that is, the quantities plotted are $\xi\partial I_{\mathrm{toa}}/\partial\xi$.

Weighting function output is useful for looking at retrieval sensitivity. For example in Fig. 7, weighting functions in the third and sixth panels are very similar in distribution. This indicates that it would be hard to distinguish the effects of the two parameters in a retrieval situation; fitting

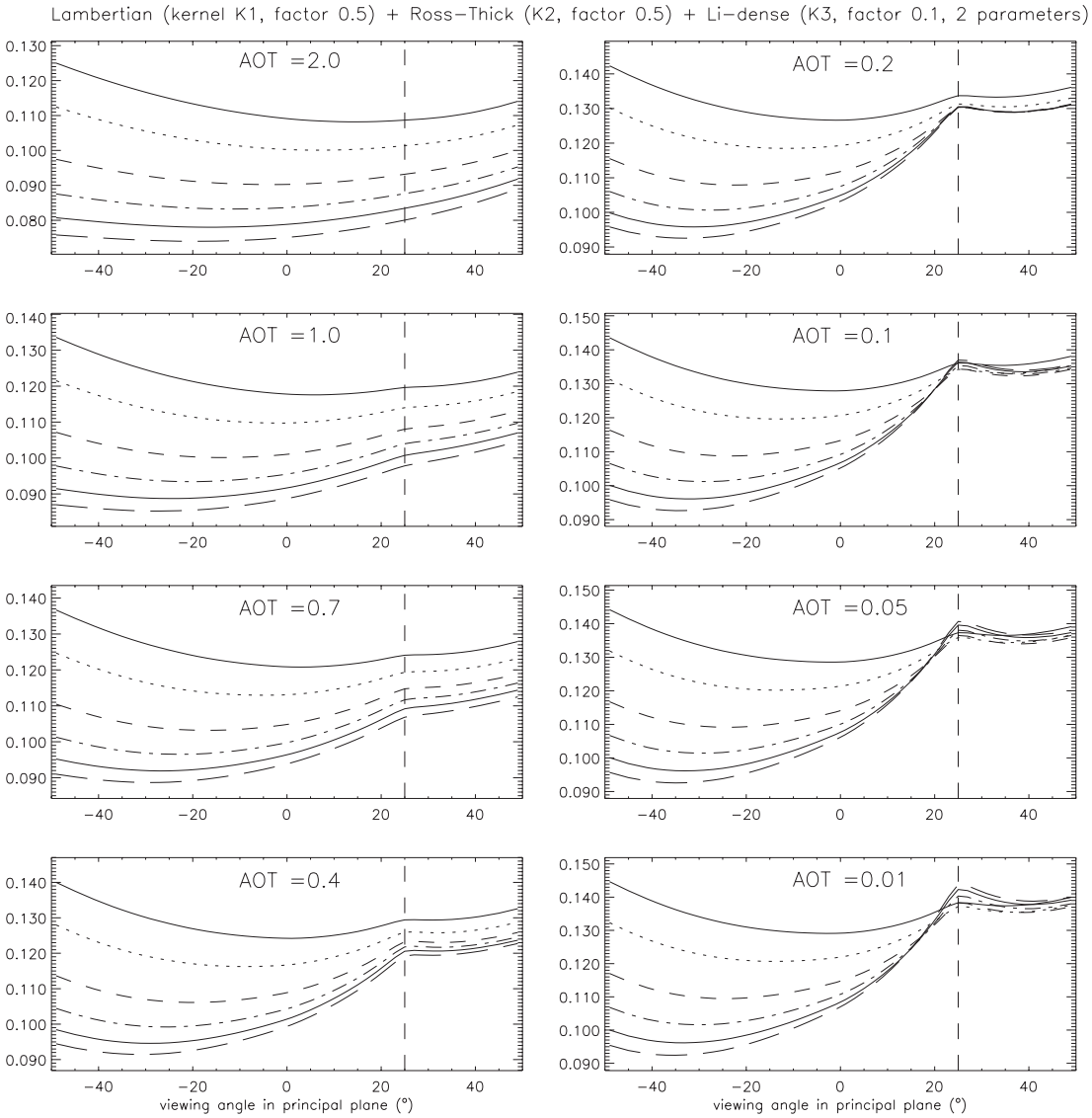

Fig. 4. Values of TOA backscatter intensity for a linear combination of BRDF kernels; a Lambertian function with linear factor 0.5, a Ross-thick function with linear factor 0.5, and a Li-dense function with linear factor 0.1 and non-linear parameters 2.5 and 2.0. Wavelengths and solar zenith angle as in previous two figures. This combination is one of the MODIS options.

PBL aerosol single scatter albedo and refractive index is not a good idea. On the other hand, all weighting functions with respect to wind speed (Fig. 7 panel 5 and Fig. 9 panel 6) have distinctive shapes not seen in other sensitivity functions, indicating that this quantity can be retrieved with some confidence.

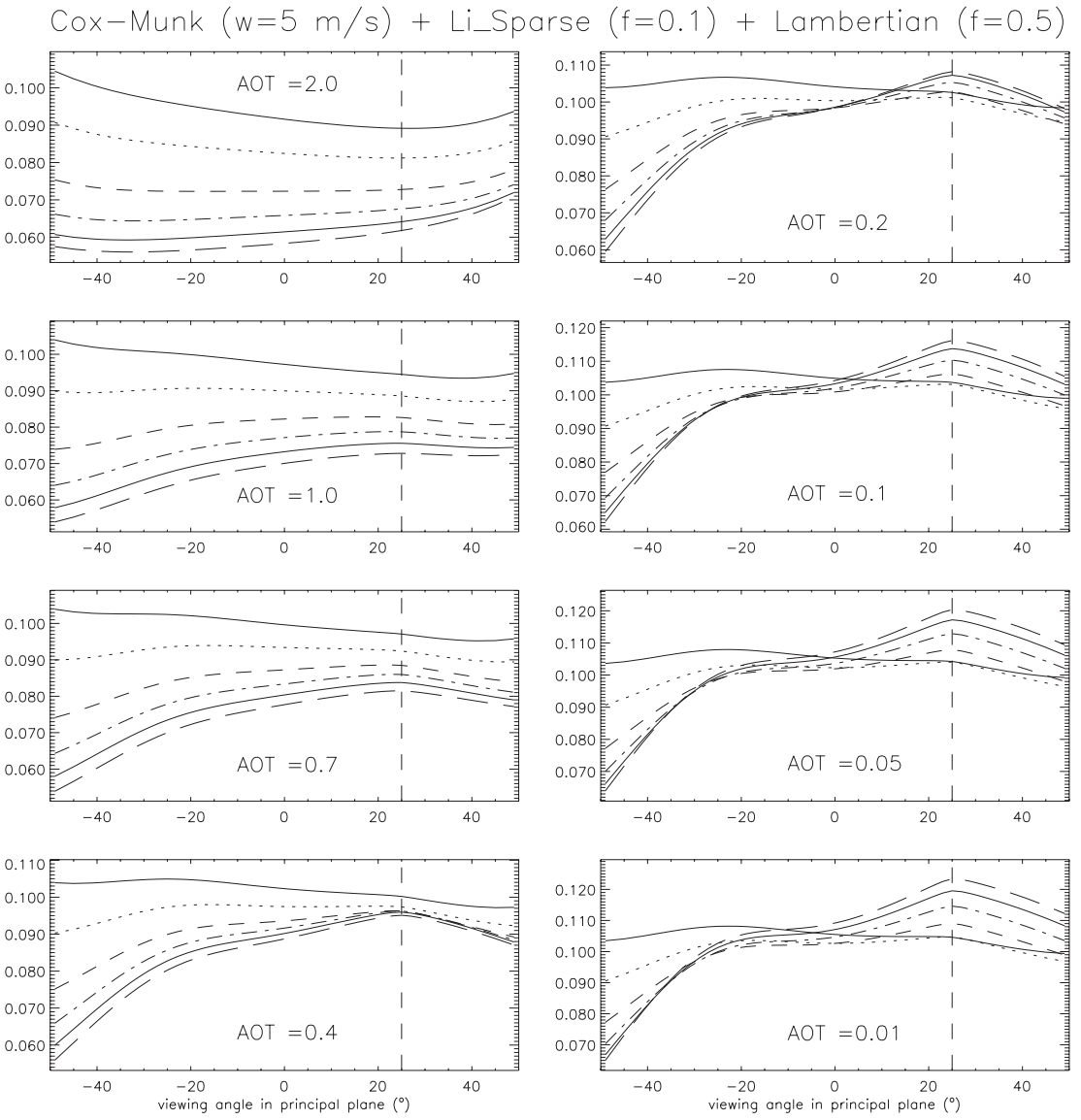

Fig. 5. Values of TOA backscatter intensity for a linear combination of BRDF kernels; a Lambertian function with linear factor 0.5, a Cox–Munk function with linear factor 1.0 and parameters 5.0 and 1.334 as in Fig. 3, and a Li-sparse function with linear factor 0.1 and non-linear parameters 1.0 and 2.0. Wavelengths and solar zenith angle as in previous three figures. This combination is the MODIS option for vegetation cover with a surface water component.

4.4. Self-consistent surface property retrieval

In this section we look beyond pure RT model output and attempt some fitting. Synthetic measurements in the form of sun-normalized radiances I_s are created using the LIDORT model in

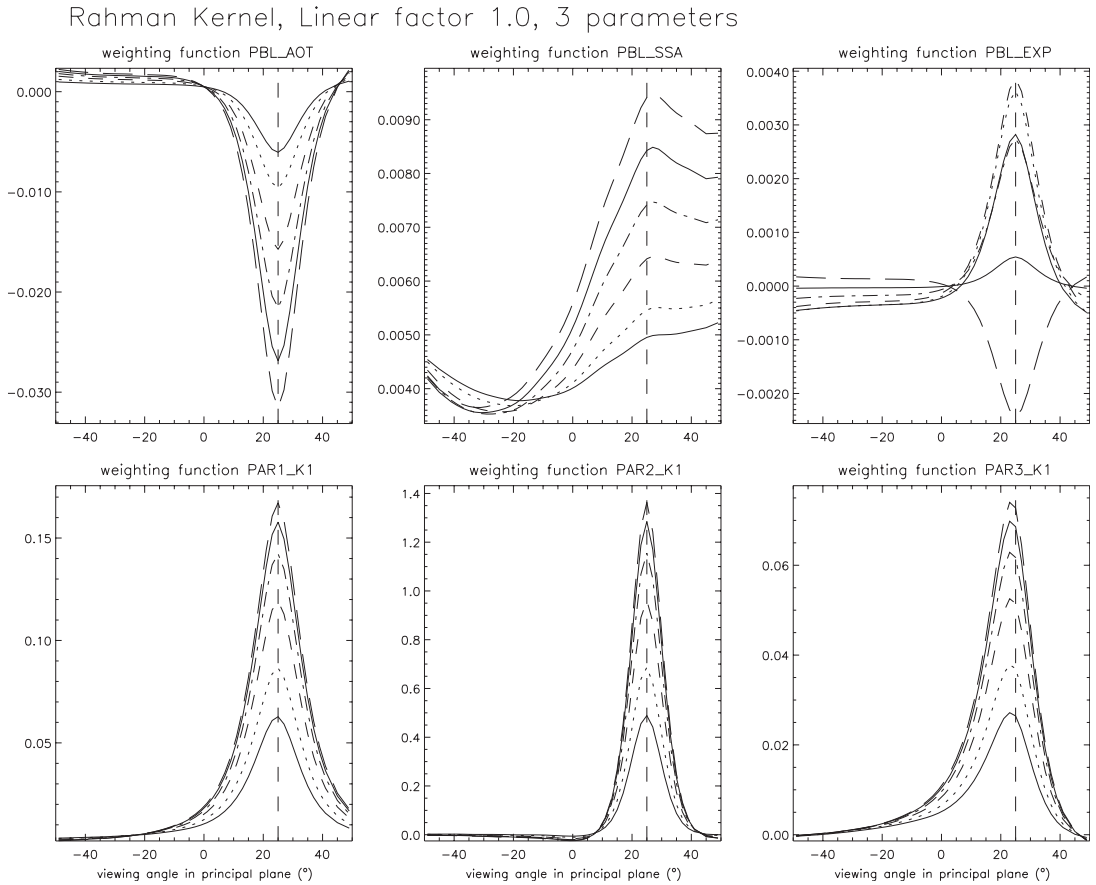

Fig. 6. Values of TOA backscatter weighting functions for the Rahman BRDF kernel with linear factor 1.0, and non-linear parameters 0.1, −0.8 and 1.5 as in Fig. 2. The AOT is 0.1. The three PBL aerosol weighting functions are in the top 3 panels, while the lower panels are surface weighting functions for the non-linear kernel parameters. The scale factor weighting function is not shown.

"intensity-only" mode (no Jacobians) for a given set of atmospheric and surface parameters. We assume independent Gaussian statistics for errors on these synthetic measurements, with error levels set at $\varepsilon_3 \equiv 10^{-3}$ and $\varepsilon_4 \equiv 10^{-4}$. Synthetic measurements were created at 5 of the 6 wavelengths used in the previous two sections (590 nm was left out), and for a set of 23 viewing angles from 1° to 41° at intervals of 2°, plus two additional measurements at 45° and 49°. We consider measurements in both solar and anti-solar planes; all told, there are 230 multi-angle measurements for a given scenario and solar zenith angle. We pick the MODIS-type scenario with a vegetation cover and surface water: Figs. 5 and 9 in the previous section.

For the fitting, we use the standard optimal estimation method, which proceeds iteratively in a series of linear inversion steps as noted in Eq. (2). Since we are using the same RT in the forward model as was used to create synthetic measurements, the fitting should converge to the "truth" values that were used in the synthetic measurement simulation, subject of course to retrieval

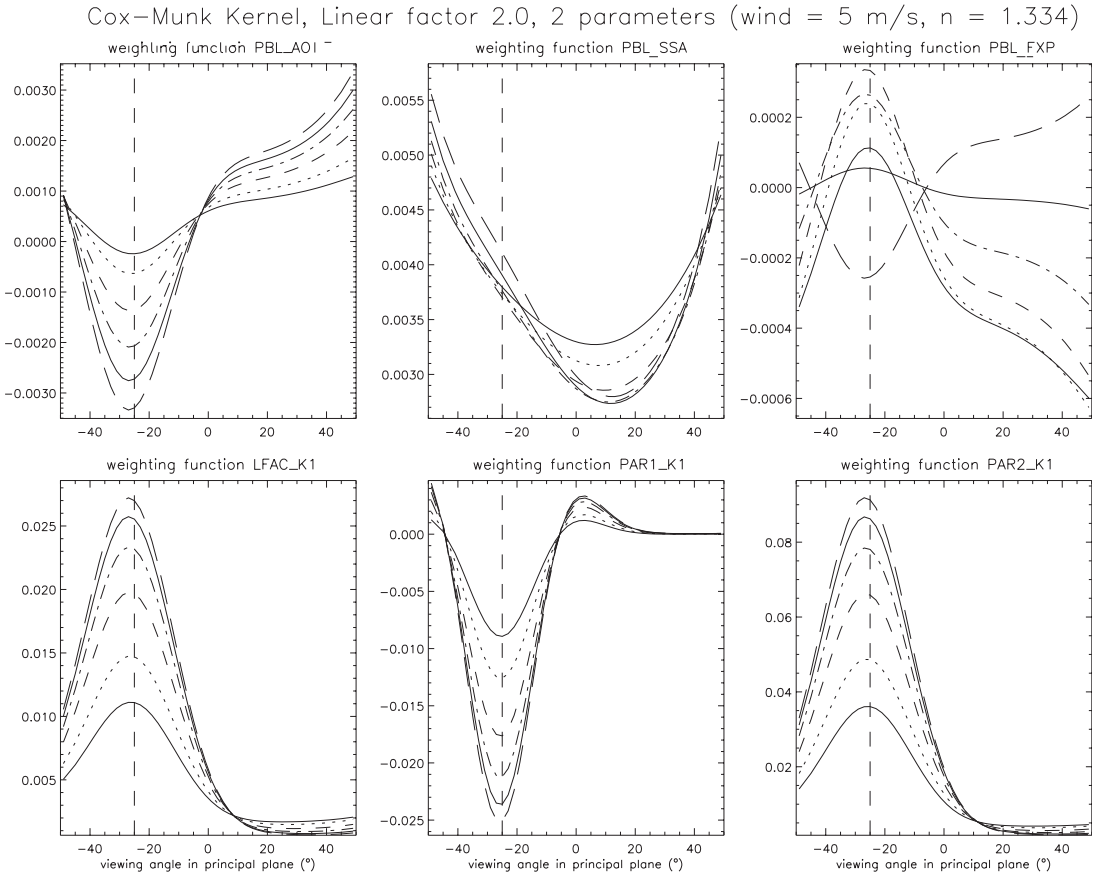

Fig. 7. Values of TOA backscatter weighting functions for the single Cox–Munk BRDF kernel with linear factor 2.0, and non-linear parameters 5.0 (wind speed in m/s) and 1.334 (refractive index). The lower center panel has the wind speed weighting functions.

uncertainty. The retrieval is perfect if there are no other sources of error. We can create a more realistic situation by introducing two other error sources: (1) some random noise on the synthetic measurements, via $I'_s = I_s + \varepsilon_3 \cdot G_s$ or $I'_s = I_s + \varepsilon_4 \cdot G_s$, where G_s is a Gaussian random deviate; and (2) some forward model error by using LIDORT with a lower number of discrete ordinates in the retrieval. For the results in Tables 1–3, 14 half-space streams were used for the synthetic measurements, and 7 streams were used for LIDORT in the retrieval. Another source of error is model parameter uncertainty (for example, knowledge of the temperature profile); we do not consider this here, other than to note that it is straightforward to include it in the fitting as long as some statistics are present and provided the appropriate sensitivity functions can be conveniently calculated. In this regard, the latter aspect is easily dealt with by LIDORT, which has a full weighting function capability.

We use a global fit with all 230 observations. In a sense this is an example of hyperspectral image fitting; the aim is to combine multi-angle observations at a number of spectral channels to determine

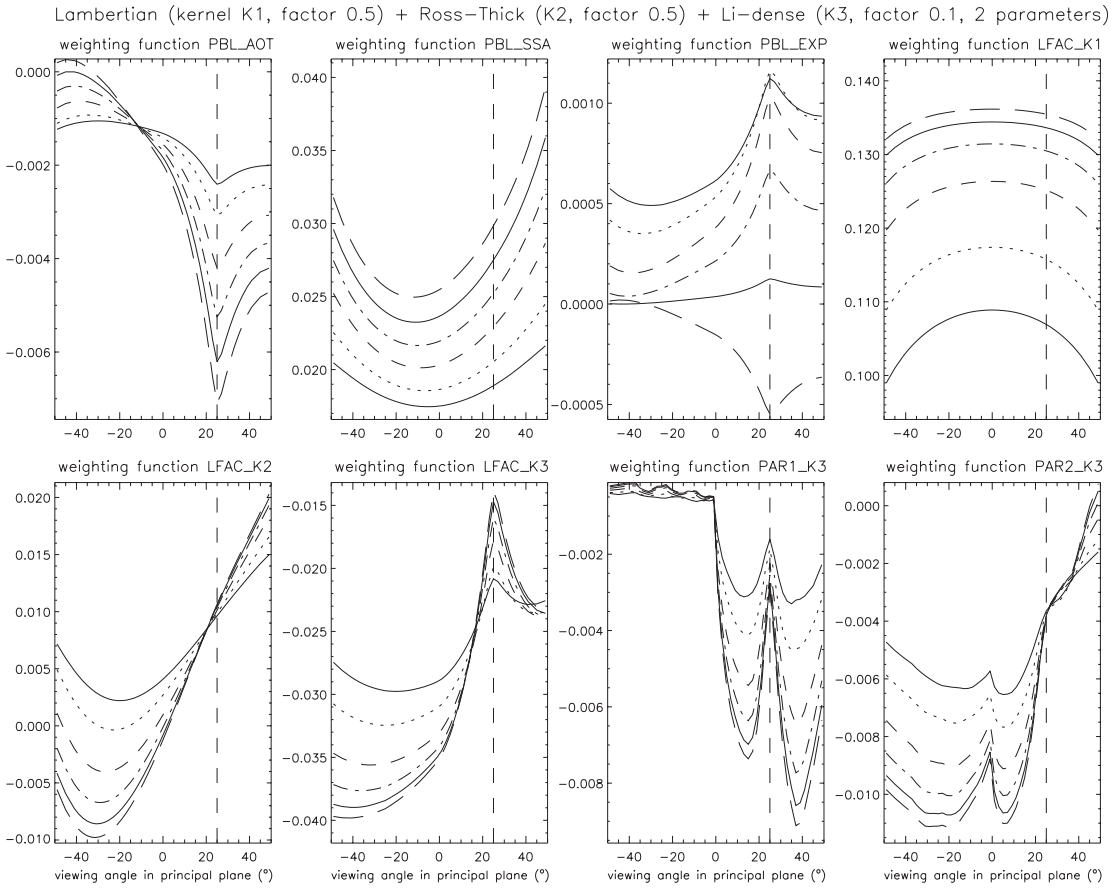

Fig. 8. TOA backscatter weighting functions for the linear combination of BRDF kernels in Fig. 4; total of 8 weighting functions (3 atmospheric, 5 surface).

a whole range of surface and lower atmosphere parameters. This is just the sort of situation that applies to MODIS; this kind of global fit has (to my knowledge) not been attempted yet for this instrument. For the scenario considered, there are 3 kernels (Lambertian, Cox–Munk and Li-sparse). For the state vector, we try to retrieve all 3 aerosol parameters, all 3 linear kernel coefficients and 3 out of the 4 non-linear kernel parameters (we omit the refractive index of water). There are 9 parameters in all. For all parameters, the initial guess was taken to be 25% away from the true value. Retrieval accuracy is examined by looking at the solution covariance matrix. The initial guess was also taken to be the *a priori* state vector; in this rather idealized case, the fitting is not ill-conditioned, and it is only necessary to impose light regularization (100% standard deviations and no cross-correlations for the *a priori* covariance).

Tables 1 and 2 summarize two global fits for this scenario, with "true" values compared alongside *a priori* and retrieved values, and the retrieval parameter standard deviation (square roots of the diagonal entries in the solution covariance matrix). Also shown are the % departures of the retrieved

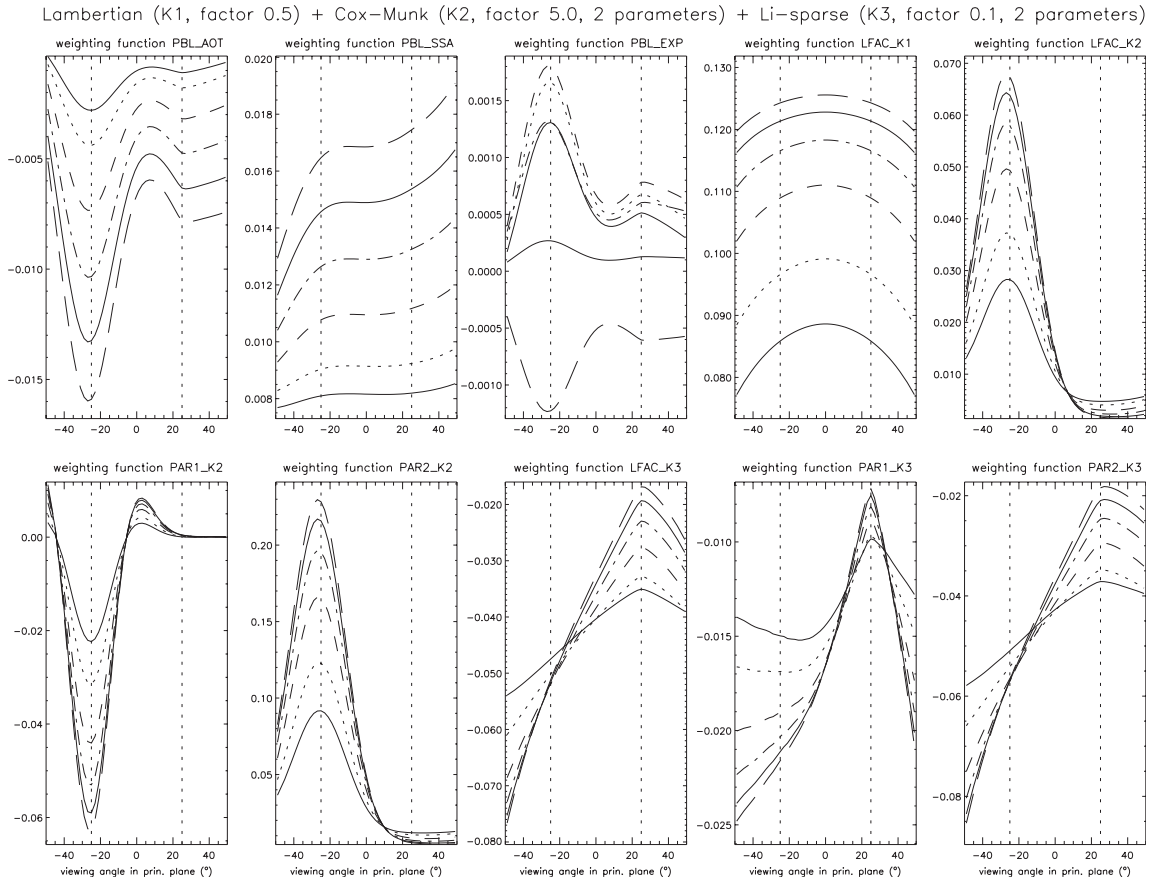

Fig. 9. TOA backscatter weighting functions for the linear combination of BRDF kernels in Fig. 5; total of 10 weighting functions (3 atmospheric, 7 surface).

values from the truth. Fit results reflect the influence of forward model errors as noted above, and the inclusion of random errors. Table 1 is based on a general noise level of ε_3, Table 2 on ε_4. For UV and visible backscattered light at the wavelengths noted here, these noise levels are realistic for solar zenith angle 25°. In both cases, 6 iterations were required for convergence. In optimal estimation one can define the degrees-of-freedom of signal and the total information diagnostics, DFS and H, respectively; for details see [3]. As expected, the DFS was close to 9.0 (the dimension of state vector space); for the information, $H = 54.37$ for the ε_3 case (Table 1), with $H = 75.10$ for the ε_4 case (Table 2).

Also of interest is the cross-correlation matrix which corresponds to the off-diagonal entries in the solution covariance. An example is given in Table 3 for the same retrieval problem; we notice in general that there are no correlations close to 1 or -1, with one exception. Parameters 7 and 9 (the Li-sparse kernel linear coefficient and second aspect ratio) are highly anti-correlated, indicating that there will be little to distinguish them in practice. In this respect, the wind speed and the PBL aerosol optical thickness are noticeably “easy” quantities to recover.

Table 1
Self-consistent optimal estimate retrieval for 9 surface and PBL aerosol properties as indicated

Parameter	*A priori*	Truth	Retrieved	Accuracy (% difference)	Departure (% difference)
PBL optical thickness	0.1250	0.1000	0.09792	1.98699	−2.08290
PBL single scatter albedo	0.9000	0.8500	0.84454	2.11441	−0.64191
PBL Angstrom exponent	1.3750	1.1000	1.16772	4.11372	6.15603
Kernel 1, linear coeff.	0.6250	0.5000	0.49966	0.21687	−0.06798
Kernel 2, linear coeff.	6.2500	5.0000	4.94776	0.57176	−1.04483
Kernel 2, Wind speed (m/s)	7.5000	5.0000	4.98037	0.30527	−0.39258
Kernel 3, linear coeff.	0.1250	0.1000	0.10261	2.06136	2.60710
Kernel 3, aspect ratio h/r	1.2500	1.0000	0.98704	0.96210	−1.29550
Kernel 3, aspect ratio h/b	2.5000	2.0000	1.95089	1.90004	−2.45538

Kernel 1 is Lambertian, kernel 2 is Cox–Munk, kernel 3 is Li-sparse. Noise level $\varepsilon_3 = 1.0^{-3}$. Fit includes forward model error (7 streams in the retrieval as opposed to 14 streams in the synthetic calculation). Global fit with 230 observations, solar zenith angle 25°.

Table 2
Self-consistent optimal estimate retrieval, for scenario as in previous table, but with noise level $\varepsilon_4 = 1.0^{-4}$

Parameter	*A priori*	Truth	Retrieved	Accuracy (% difference)	Departure (% difference)
PBL optical thickness	0.1250	0.1000	0.09945	0.19316	−0.54660
PBL single scatter albedo	0.9000	0.8500	0.84585	0.21234	−0.48782
PBL Angstrom exponent	1.3750	1.1000	1.11525	0.42174	1.38631
Kernel 1, linear coeff.	0.6250	0.5000	0.50048	0.02284	0.09512
Kernel 2, linear coeff.	6.2500	5.0000	4.99360	0.05799	−0.12797
Kernel 2, linear coeff.	7.5000	5.0000	4.99963	0.03042	−0.00742
Kernel 3, linear coeff.	0.1250	0.1000	0.10066	0.20813	0.65640
Kernel 3, aspect ratio h/r	1.2500	1.0000	0.99756	0.09386	−0.24425
Kernel 3, aspect ratio h/b	2.5000	2.0000	1.98897	0.19498	−0.55154

It is clear from Fig. 5 that surface information is lost for higher values of PBL AOT. This is a critical issue for the successful retrieval of surface quantities, and the PBL AOT along with solar zenith angle are the two main determinants here. We may look at this in our idealized case by carrying out the retrieval for a number of values of the PBL AOT. Results shown in Table 4 were carried out with a 10-stream discretization for both synthetic and forward model simulations to avoid ambiguity due to the presence of forward model errors. It is immediately clear that the critical AOT value is around 0.87; for values higher than this, the fitting settles on the "wrong values". The new fitted PBL values are a few percent off the truth, as are the parameters for the Lambertian and Cox–Munk kernels. The three Li-sparse quantities (state vector elements 7, 8 and 9) are completely wrong for AOT > 0.87; information on this kernel is lost.

Table 3
Correlation matrix for self-consistent optimal estimate retrieval, for scenario as in previous tables, with noise level $\varepsilon_4 = 1.0^{-4}$

Parameter number								
1	2	3	4	5	6	7	8	9
1.0000	0.6036	−0.5233	−0.0331	0.5668	−0.0666	−0.0440	0.2779	0.0851
0.6036	1.0000	0.2288	−0.7913	0.0681	−0.2136	0.3677	0.0129	−0.3755
−0.5233	0.2288	1.0000	−0.6570	−0.5086	−0.0266	0.4312	−0.3418	−0.4624
−0.0331	−0.7913	−0.6570	1.0000	0.4664	0.3919	−0.6358	0.3935	0.6683
0.5668	0.0681	−0.5086	0.4664	1.0000	0.7457	−0.7733	0.8293	0.8005
−0.0666	−0.2136	−0.0266	0.3919	0.7457	1.0000	−0.7963	0.7386	0.7954
−0.0440	0.3677	0.4312	−0.6358	−0.7733	−0.7963	1.0000	−0.8053	−0.9960
0.2779	0.0129	−0.3418	0.3935	0.8293	0.7386	−0.8053	1.0000	0.7860
0.0851	−0.3755	−0.4624	0.6683	0.8005	0.7954	−0.9960	0.7860	1.0000

Table 4
Effect of PBL aerosol optical thickness (column 1) on retrieval

AOT truth	% deviations from truth for parameter number								
	1	2	3	4	5	6	7	8	9
0.500	−0.0387	−0.0085	0.0895	−0.0317	−0.1448	−0.0660	0.3914	−0.2004	−0.3942
0.700	−0.0313	−0.0117	0.0512	−0.0387	−0.1712	−0.0777	0.4711	−0.2554	−0.4789
0.800	−0.0238	−0.0114	0.0325	−0.0369	−0.1660	−0.0777	0.4336	−0.2481	−0.4469
0.850	−0.0197	−0.0109	0.0235	−0.0341	−0.1592	−0.0773	0.3922	−0.2323	−0.4091
0.870	−0.0177	−0.0106	0.0204	−0.0330	−0.1566	−0.0773	0.3803	−0.2273	−0.3978
0.875	1.4607	0.7854	0.4072	3.3291	5.6334	4.0859	−44.835	24.627	87.201
0.900	1.2579	0.7473	0.6456	3.2545	5.3689	4.0934	−44.726	24.374	86.628
1.000	0.4688	0.6260	1.4914	2.9480	3.8439	4.0582	−45.781	24.538	89.165
1.200	−1.0295	0.4785	3.0885	2.0180	0.2613	4.1207	−48.621	25.034	96.483
1.500	−2.5606	0.3490	4.5647	0.4787	−5.4670	3.6082	−53.300	25.345	110.36

Random noise only at the ε_4 level.

5. Concluding remarks

In this paper we have shown that in a multi-layer anisotropically scattering atmospheric medium, quasi-analytic and accurate weighting functions with respect to a very general set of surface properties can be computed efficiently without recourse to unnecessary approximations. The required theory was developed for the linearized discrete ordinate radiative transfer model LIDORT. For remote sensing applications, the efficient and accurate generation of surface property radiance sensitivities allows the retrieval to be done in a direct manner using standard non-linear inversion techniques, without the need for two-step approximate procedures based on expediency.

Results of simulated radiances and surface property weighting functions were shown for a number of surface scenarios parameterized semi-empirically with various volume-scattering and surface-optics

models, and also for the characteristic specular glitter BRDF kernel. Weighting functions were also shown for a 3-parameter model of the planetary boundary layer aerosol—this constituent is the largest source of error in surface property retrieval. It was shown that global fitting of multi-angle backscatter measurements at a few spectral channels is feasible, allowing for the simultaneous retrieval of PBL parameters alongside the desired surface properties.

Although the discussion was focussed on the linear BRDF kernel combinations typifying surface property retrieval from the MODIS and POLDER instruments, the linearization treatment in LIDORT is generic, and the model can be used to derive accurate sensitivity functions for any number of surface and atmospheric properties. In the next paper, I intend to use this combination of LIDORT in conjunction with a global fitting technique to retrieve surface and aerosol information from real MODIS backscatter data.

Acknowledgements

The author would like to thank Roeland van Oss and Knut Stamnes for stimulating discussions on this work.

Appendix A.

We list here the 8 non-Lambertian BRDF kernels used in this work. We do not attempt to derive these semi-empirical models from scratch, instead referring the reader to the literature. However, we derive partial derivatives with respect to those non-linear parameters which affect the kernel shapes.

A.1. Roujean kernel

This was derived from a consideration of the reflectance of a random arrangement of rectangular blocks on a flat surface [12]. The kernel has no free parameters and is given by

$$f_{\text{roujean}}(\theta_i, \theta_r, \phi) = [(\pi - \phi)\cos\phi + \sin\phi]\tan\theta_i \tan\theta_r - \Delta(\theta_i, \theta_r, \phi), \tag{A.1}$$

with

$$\Delta(\theta_i, \theta_r, \phi) = \frac{1}{\pi}\{\tan\theta_i + \tan\theta_r + \sqrt{\tan^2\theta_i + \tan^2\theta_r - 2\tan\theta_i \tan\theta_r \cos\phi}\}.$$

A.2. Li-sparse and Li-dense kernels

These kernels apply to reflectances modeled for vegetation cover; they are derived from consideration of the proportional areas of sunlit tree crowns and sunlit ground for randomly distributed cover. Kernel differences depend on the treatment of mutual shadowing. Tree crowns are assumed to be spheroids of vertical dimension b, horizontal dimension r, with their centers at height h above the ground. There are two free parameters characterizing the kernels, namely the "crown ratio" $x = b/r$

and the "height ratio" $y = h/b$. Derivations for these kernels may be found in the work of Wanner et al. [11] and references therein. We may write them as

$$f_{\text{sparse}}(x, y) = \tfrac{1}{2}\, p(x) - q(x, y) r(x), \tag{A.2}$$

$$f_{\text{dense}}(x, y) = \frac{p(x)}{q(x, y) r(x)} - 2, \tag{A.3}$$

where

$$p(x) = (1 + \cos\xi')b(x),$$

$$q(x, y) = 1 - \frac{1}{\pi}(t - \sin t \cos t),$$

$$r(x) = a(x) + b(x),$$

$$a(x) = \sec\theta_i', \quad b(x) = \sec\theta_r',$$

$$\cos\xi' = \cos\theta_i' \cos\theta_r' + \sin\theta_i' \sin\theta_r' \cos\phi,$$

$$r(x)\cos t = y h(x),$$

$$h(x) = \sqrt{d^2(x) + \tan^2\theta_i' \tan^2\theta_r' \sin^2\phi},$$

$$d(x) = \sqrt{\tan^2\theta_i' + \tan^2\theta_r' + 2\tan\theta_i' \tan\theta_r' \cos\phi},$$

$$\tan\theta_i' = x \tan\theta_i, \quad \tan\theta_r' = x \tan\theta_r.$$

The angular dependence has been dropped for clarity. If there is no overlap area, then $q(x, y) \equiv 1$. Note that both functions are identically zero when the angle of incidence equals the angle of reflection in the principal plane $\phi = 0$. It is straightforward to find the derivatives. We have

$$\frac{\partial f_{\text{sparse}}}{\partial x} = \frac{1}{2}\frac{\partial p}{\partial x} - \frac{\partial q}{\partial x} r - q\frac{\partial r}{\partial x}, \tag{A.4}$$

$$\frac{\partial f_{\text{dense}}}{\partial x} = (f_{\text{dense}} + 2)\left[\frac{1}{p}\frac{\partial p}{\partial x} - \frac{1}{r}\frac{\partial r}{\partial x} - \frac{1}{q}\frac{\partial q}{\partial x}\right], \tag{A.5}$$

and

$$\frac{\partial f_{\text{sparse}}}{\partial y} = -\frac{\partial q}{\partial y} r, \tag{A.6}$$

$$\frac{\partial f_{\text{dense}}}{\partial y} = -(f_{\text{dense}} + 2)\frac{1}{q}\frac{\partial q}{\partial y}. \tag{A.7}$$

The auxiliary functions $p(x)$, $q(x,y)$ and $r(x)$ are common to both kernels, and their derivatives may be obtained by differentiation of the above. We find

$$\frac{\partial r}{\partial x} = \frac{r}{x}\left(1 - \frac{1}{ab}\right),$$

$$\frac{\partial p}{\partial x} = \frac{1}{xa^2}\left\{p(1+a^2) - \frac{r^2}{b}\right\},$$

$$\frac{\partial q}{\partial x} = \frac{2}{\pi}\sin t \cos t \left[\frac{1}{h}\frac{\partial h}{\partial x} - \frac{1}{r}\frac{\partial r}{\partial x}\right],$$

$$\frac{\partial q}{\partial y} = \frac{2}{\pi y}\sin t \cos t,$$

$$\frac{\partial h}{\partial x} = \frac{2h^2 - d^2}{hx}.$$

A.3. Ross-thin and Ross-thick kernels

These reflectance kernels are based on volume-scattering empirical models, in which a radiative transfer model is applied to randomly oriented scattering facets (leaves) over a flat surface of known Lambertian albedo. The kernels have no degrees of freedom (no non-linear parameters). Following the definitions in Wanner et al. [11], we have

$$f_{\text{thick}}(\theta_i, \theta_r, \phi) = \frac{(\pi/2 - \xi)\cos\xi + \sin\xi}{\cos\theta_i + \cos\theta_r} - \frac{\pi}{4}, \tag{A.8}$$

$$f_{\text{thin}}(\theta_i, \theta_r, \phi) = \frac{(\pi/2 - \xi)\cos\xi + \sin\xi}{\cos\theta_i \cos\theta_r} - \frac{\pi}{2}, \tag{A.9}$$

where

$$\cos\xi = \cos\theta_i \cos\theta_r + \sin\theta_i \sin\theta_r \cos\phi.$$

A.4. Hapke kernel

This kernel was developed in the work of Hapke [14]. There are 3 parameters characterizing the kernel. In terms of the cosines $\mu_i = \cos\theta_i$ and $\mu_r = \cos\theta_r$ we have

$$f_{\text{hapke}}(\theta_i, \theta_r, \phi) = R_{ir}\{(1 + B(\xi))P(\xi) + T_i T_r - 1\}, \tag{A.10}$$

where

$$R_{ir} = \frac{\Omega}{4(\mu_i + \mu_r)},$$

$$\cos\xi = \cos\theta_i \cos\theta_r + \sin\theta_i \sin\theta_r \cos\phi,$$

$$\boldsymbol{P}(\xi) = 1 + \tfrac{1}{2}\cos\xi,$$

$$\boldsymbol{B}(\xi) = \frac{B_0 \Delta}{\Delta + \tan(1/2)\xi},$$

$$T_i = \frac{1 + 2\mu_i}{1 + 2\mu_i \Gamma},$$

$$T_r = \frac{1 + 2\mu_r}{1 + 2\mu_r \Gamma},$$

$$\Gamma = \sqrt{1 - \Omega}.$$

The free parameters are Ω (single scattering albedo), B_0 (amplitude of the hot-spot), and Δ (angular width of the hot-spot). Derivatives are straightforward; we have

$$\frac{\partial f_{\text{hapke}}}{\partial \Omega} = \frac{f_{\text{hapke}}}{\Omega} + R_{ir}\frac{\partial (T_i T_r)}{\partial \Omega}, \tag{A.11}$$

$$\frac{\partial f_{\text{hapke}}}{\partial \Delta} = \frac{R_{ir} P(\xi) B(\xi)}{\Delta}\left[1 - \frac{B(\xi)}{B_0}\right], \tag{A.12}$$

$$\frac{\partial f_{\text{hapke}}}{\partial B_0} = \frac{R_{ir} P(\xi) B(\xi)}{B_0}, \tag{A.13}$$

with

$$\frac{\partial T_i}{\partial \Omega} = \frac{\mu_i T_i}{\Gamma(1 + 2\mu_i \Gamma)} \quad \text{and} \quad \frac{\partial T_r}{\partial \Omega} = \frac{\mu_r T_r}{\Gamma(1 + 2\mu_r \Gamma)}$$

A.5. Rahman model

This empirical model [13] includes an explicit form for the phase function of the surface distribution of scatterers in the form of a Henyey–Greenstein function with asymmetry parameter γ_1 (which is one of the three non-linear parameters characterizing the BRDF kernel). The other two parameters are γ_2, which determines the angular spread, and γ_0, which gives the overall amplitude. The hot spot function is modeled empirically. We have

$$f_{\text{rahman}}(\theta_i, \theta_r, \phi) = \gamma_0 P(\xi)[1 + R(\xi)]\left[\frac{\mu_i \mu_r}{\mu_i + \mu_r}\right]^{\gamma_2 - 1}, \tag{A.14}$$

where

$$\cos\xi = \cos\theta_i \cos\theta_r + \sin\theta_i \sin\theta_r \cos\phi,$$

$$P(\xi) = \frac{1 - \gamma_1^2}{[1 + \gamma_1^2 + 2\gamma_1 \cos\xi]^{1.5}} \quad \text{(phase function)},$$

$$R(\xi) = \frac{1 - \gamma_0}{1 + \Delta} \quad \text{(hot-spot function)}.$$

where $\Delta = \Delta(\theta_i, \theta_r, \phi)$ is defined as for the Roujean kernel. Derivatives of this BRDF with respect to the three parameters are:

$$\frac{1}{f_{\text{rahman}}}\frac{\partial f_{\text{rahman}}}{\partial \gamma_0} = \frac{1}{\gamma_0} - \frac{1}{[1+R(\xi)](1+\Delta)}, \tag{A.15}$$

$$\frac{1}{f_{\text{rahman}}}\frac{\partial f_{\text{rahman}}}{\partial \gamma_1} = -\frac{2\gamma_1}{1-\gamma_1^2} - \frac{3}{2}\frac{2\gamma_1 + 2\cos\xi}{[1+\gamma_1^2+2\gamma_1\cos\xi]}, \tag{A.16}$$

$$\frac{1}{f_{\text{rahman}}}\frac{\partial f_{\text{rahman}}}{\partial \gamma_2} = \ln\left[\frac{\mu_i\mu_r}{\mu_i+\mu_r}\right]. \tag{A.17}$$

A.6. Cox–Munk specular kernel

This is a function representing the glitter term. We use a geometric optics model, with the usual assumption of a Gaussian distribution of the slopes of the wave facets, and the empirical relation $\sigma^2 = \alpha + \beta W$ where W is the wind speed in meters per second and σ^2 is the Gaussian spread. Cox and Munk [19] derived values of 0.003 for α and 0.00512 for β; these values are still in common use. Obviously wind speed is one free parameter; the other is the value of the refractive index of water—this is usually specified as $m = 1.334$, but its value does depend somewhat on water turbidity. The kernel is

$$f_{\text{spec}}(\theta_i, \theta_r, \phi) = R(m, \xi)P(W, \mu_i, \mu_r), \tag{A.18}$$

where the Fresnel reflection term is

$$R(m, \xi) = \frac{r_+^2 + r_-^2}{2}, \tag{A.19}$$

with

$$r_+ = \frac{m^2\lambda - c}{m^2\lambda + c},$$

$$r_- = \frac{\lambda - c}{\lambda + c},$$

$$c = \sqrt{m^2 + (\lambda^2 - 1)},$$

$$\lambda = \cos(\xi/2), \quad \text{where } \cos\xi = \cos\theta_i\cos\theta_r + \sin\theta_i\sin\theta_r\cos\phi$$

and angle ξ defined as before. The Gaussian probability function is given by

$$P(W, \theta_i, \theta_r) = \frac{1}{4\mu_i\mu_r\pi\sigma^2\gamma^4}\exp\left[\frac{-\tau^2}{\sigma^2}\right], \tag{A.20}$$

with

$$\gamma = \frac{(\mu_i + \mu_r)}{2\lambda},$$

$$\tau = \tan(\pi/2 - \sin^{-1}\gamma).$$

For derivatives with respect to W and m we have:

$$\frac{\partial f_{\text{spec}}}{\partial W} = \beta f_{\text{spec}} \frac{\sigma^2 - \tau^2}{\sigma^4}, \tag{A.21}$$

$$\frac{\partial f_{\text{spec}}}{\partial m} = 2m f_{\text{spec}} \left[r_+ \frac{\partial r_+}{\partial m^2} + r_- \frac{\partial r_-}{\partial m^2} \right], \tag{A.22}$$

with

$$\frac{\partial r_+}{\partial m^2} = \frac{\lambda(2c^2 - 1)}{c(m^2\lambda + c)^2},$$

$$\frac{\partial r_-}{\partial m^2} = -\frac{\lambda_-}{c(\lambda + c)^2},$$

References

[1] Strahler A, et al. MODIS BRDF/albedo product algorithm theoretical basis document. MOD43, Version 5.0, 1999.

[2] Bicheron P, Leroy M. Bidirectional reflectance distribution function signatures of major biomes observed from space. J Geophys Res 2000;105:26,669–81.

[3] Rodgers C. Inverse methods for atmospheric sounding. New York: World Scientific, 2000.

[4] Spurr R, Kurosu T, Chance K. A linearized discrete ordinate radiative transfer model for atmospheric remote sensing retrieval. JQSRT 2001;68:689–735.

[5] Spurr R, Simultaneous radiative transfer derivation of intensities and weighting functions in a general pseudo-spherical treatment. JQSRT, 2002;75:129–75.

[6] van Oss R, Spurr R. Fast and accurate 4 and 6 stream linearized discrete ordinate radiative transfer models for ozone profile remote sensing retrieval. JQSRT, 2001;75:177–220.

[7] Palmer P, et al. Air mass factor formulation for spectroscopic measurements from satellites: application to formaldehyde retrievals from the Global Ozone Monitoring Experiment. J Geophys Res 2001;106:14,539–50.

[8] Spurr R, Linearized radiative transfer theory: a general discrete ordinate approach to the calculation of radiances and analytic weighting functions, with application to atmospheric remote sensing. PhD thesis, Technical University of Eindhoven, Eindhoven, The Netherlands, 2001.

[9] Rozanov V, Kurosu T, Burrows J. Retrieval of atmospheric constituents in the UV/visible: a new quasi-analytical approach for the calculation of weighting functions. JQSRT 1998;60:277–99.

[10] Landgraf J, Hasekamp O, Trautmann T. Linearization of radiative transfer with respect to surface properties. JQSRT 2001;72:327–39.

[11] Wanner W, Li X, Strahler A. On the derivation of kernels for kernel-driven models of bidirectional reflectance. J Geophys Res 1995;100:21,077–90.

[12] Roujean J-L, Leroy M, Deschamps P-Y. A bidirectional model of the earth's surface for the correction of remote sensing data. J Geophys Res 1992;97:20,455–68.

[13] Rahman H, Pinty B, Verstraete M. Coupled surface atmosphere reflectance (CSAR) model: 2. Semi-empirical surface model usable with NOAA AVHRR data. J Geophys Res 1993;98:20,791–801.

[14] Hapke B. Theory of reflectance and emittance spectroscopy. Cambridge: Cambridge University Press, 1993.
[15] Stamnes K, Tsay S-C, Laszlo I. DISORT: a general purpose fortran program for discrete-ordinate-method radiative transfer in scattering and emitting layered media: documentation of methodology. NASA internal report, 2000.
[16] Thomas G, Stamnes K. Radiative transfer in the atmosphere and ocean, 1st ed. Cambridge: Cambridge University Press, 1999.
[17] Chandrasekhar S. Radiative transfer. New York: Dover Publications Inc., 1960.
[18] Chance K, Spurr R. Ring effect studies: Rayleigh scattering, including molecular parameters for rotational Raman scattering, and the Fraunhofer spectrum. Appl Opt 1997;36:5224–30.
[19] Cox C, Munk W. The measurement of the roughness of the sea surface from photographs of the Sun glitter. J Opt Soc Ann 1954;44:838–50.